https://doi.org/10.5194/tc-2019-222
Preprint. Discussion started: 26 September 2019

The Cryosphere Discussions
Open Access
EGU

21st century ocean forcing of the Greenland Ice Sheet for modeling of sea level contribution

Donald A. Slater[1], Denis Felikson[2], Fiamma Straneo[1], Heiko Goelzer[3,4], Christopher M. Little[5], Mathieu Morlighem[6], Xavier Fettweis[7], and Sophie Nowicki[2]

[1]Scripps Institution of Oceanography, University of California San Diego, La Jolla, CA, USA
[2]Cryospheric Sciences Laboratory, NASA Goddard Space Flight Center, Greenbelt, MD, USA
[3]Utrecht University, Institute for Marine and Atmospheric Research, Utrecht, the Netherlands
[4]Laboratoire de Glaciologie, Université Libre de Bruxelles, Brussels, Belgium
[5]Atmospheric and Environmental Research, Inc., Lexington, MA, USA
[6]Department of Earth System Science, University of California, Irvine, USA
[7]Laboratory of Climatology, Department of Geography, University of Liège, Liège, Belgium

Correspondence: Donald Slater (daslater@ucsd.edu)

Abstract. Changes in the ocean are expected to be an important determinant of the Greenland Ice Sheet's future sea level contribution. Yet representing these changes in continental-scale ice sheet models remains challenging due to the small scale of the key physics, and limitations in processing understanding. Here we present the ocean forcing strategy for Greenland Ice Sheet models taking part in the Ice Sheet Model Intercomparison Project for CMIP6 (ISMIP6), the primary community effort to provide 21st century sea level projections for the Intergovernmental Panel on Climate Change 6th Assessment Report. Beginning from global atmosphere-ocean general circulation models, we describe two complementary approaches to provide ocean boundary conditions for Greenland Ice Sheet models, termed the 'retreat' and 'submarine melt' implementations. The retreat implementation parameterizes glacier retreat as a function of projected submarine melting, is designed to be implementable by all ice sheet models, and results in retreat of around 1 and 15 km by 2100 in RCP2.6 and 8.5 scenarios respectively. The submarine melt implementation provides estimated submarine melting only, leaving the ice sheet model to solve for the resulting calving and glacier retreat, and suggests submarine melt rates will change little under RCP2.6 but will approximately triple by 2100 under RCP8.5. Both implementations have necessarily made use of simplifying assumptions and poorly-constrained parameterisations and as such, further research on submarine melting, calving and fjord-shelf exchange should remain a priority. Nevertheless, the presented framework will allow an ensemble of Greenland Ice Sheet models to be systematically and consistently forced by the ocean for the first time, and should therefore result in a significant improvement in projections of the Greenland ice sheet's contribution to future sea level change.

1 Introduction

The rapid response of the Greenland Ice Sheet to climate warming in the past few decades, together with expectations of future climate change, have raised concern that Greenland will contribute significantly to sea level changes over the coming decades and centuries (Shepherd et al., 2012; Church et al., 2013; Nick et al., 2013). Greenland has already contributed ∼13.7 mm to

https://doi.org/10.5194/tc-2019-222
Preprint. Discussion started: 26 September 2019

global mean sea level since 1972, with surface mass balance comprising 35-60% of this contribution, depending on the time period considered (van den Broeke et al., 2016; Mouginot et al., 2019). The remainder derives from discharge from tidewater outlet glaciers, most of which have retreated, accelerated and thinned in recent decades (Rignot and Kanagaratnam, 2006; Khan et al., 2014; Murray et al., 2015). These changes at outlet glaciers are understood to have been in response to climate forcing occurring at calving fronts, where the ice sheet meets the ocean (Nick et al., 2009; Luckman et al., 2015; Wood et al., 2018). Thus ocean forcing of Greenland Ice Sheet models, which forms the focus of this paper, is a critical component of accurate future sea level projections.

The Ice Sheet Model Intercomparison Project for CMIP6 (ISMIP6; Nowicki et al., 2016) seeks to produce projections of future sea level contribution from the Greenland and Antarctic Ice Sheets for the coming 6th Assessment Report of the Intergovernmental Panel on Climate Change (IPCC AR6). ISMIP6 follows a history of similar initiatives, such as SeaRISE (Bindschadler et al., 2013; Nowicki et al., 2013a, b) and ice2sea (Gillet-Chaulet et al., 2012; Goelzer et al., 2013), aimed at bringing together a number of ice sheet models and scientists across disciplines to improve projections of ice sheet mass loss. Compared to previous initiatives, ISMIP6 is the first such effort to be fully integrated within the Coupled Model Intercomparison Project (CMIP), meaning that the ice sheet models will be systematically forced by a subset of the climate model output that is used throughout the IPCC assessment reports. Full details of the ISMIP6 project can be found in Nowicki et al. (2016) and on the ISMIP6 webpage (http://www.climate-cryosphere.org/activities/targeted/ismip6). This paper focuses specifically on one aspect of ISMIP6: the representation of ocean forcing in models of the Greenland Ice Sheet. The aim is to relate large-scale climate – as defined by the CMIP coupled Atmosphere and Ocean general circulation models (AOGCMs) – to an ocean boundary condition for the ice sheet models.

Ocean forcing of the Greenland Ice Sheet (here broadly defined as the impact of varying ocean properties on submarine melting and glacier retreat) occurs at around 300 approximately vertical glacier calving fronts, and a handful of larger ice shelves located in northern Greenland. The processes, challenges, and decisions involved in the design of such an ocean forcing are numerous. First, in order to drive melting of calving fronts, heat must be sourced from the far-field ocean, across continental shelves and up long and narrow fjords, processes which are not captured by AOGCMs or indeed current regional ocean models. Second, submarine melting is understood to be enhanced in summer by the emergence of subglacial runoff from beneath tidewater glaciers, so that surface melting of the ice sheet contributes to ocean forcing. Third, due to computational expense and a lack of process understanding, continental-scale ice sheet models struggle to simulate the impact of ocean forcing on calving and glacier retreat. Each of these issues must be considered in the design of ocean forcing for Greenland Ice Sheet models.

To date, attempts to project future ice discharge from tidewater glaciers have often relied on extrapolation from a few glaciers to the whole ice sheet (Nick et al., 2013; Goelzer et al., 2013; Peano et al., 2017; Morlighem et al., 2019; Beckmann et al., 2019), or have employed ad-hoc methods to mimic the impact of ocean forcing that are not easily relatable to climate warming scenarios (Price et al., 2011; Fürst et al., 2015; Bindschadler et al., 2013). In a single ice sheet model, a significant advance was recently made by Aschwanden et al. (2019), who ran full ice sheet projections that resolve tidewater glaciers and were forced

https://doi.org/10.5194/tc-2019-222
Preprint. Discussion started: 26 September 2019

by estimated submarine melt rates. Here we present a strategy for simulating the impact of the ocean on the ice sheet that will enable a suite of Greenland Ice Sheet models of diverse capability to be systematically forced by future warming scenarios.

Slater et al. (2019) described the motivation, design and calibration of a tidewater glacier retreat parameterisation in addition to providing a brief example projection. The present paper is complementary in that it details the application of the retreat parameterisation within the ISMIP6 framework, focuses on the future projections across the CMIP AOGCM ensemble, and details a second, more sophisticated ocean forcing option available to ice sheet models taking part in ISMIP6. The paper proceeds as follows. An overview of the two-tier strategy for ocean forcing is first given, before the preparation of subglacial runoff and ocean thermal forcing datasets is described. The combination of these time series into projections of glacier retreat and submarine melting is illustrated. We finally discuss the projected ocean forcing, its temporal evolution, and spatial and inter-model variability.

2 Methods

2.1 Overview

Over the past decade there has been a growing recognition of the impact of the ocean on the Greenland Ice Sheet. Warming of the North Atlantic in the late 1990s was followed by rapid retreat, acceleration and thinning of tidewater glaciers around the ice sheet (Straneo and Heimbach, 2013; Murray et al., 2015). More detailed site-specific studies have since shown that offshore warm Atlantic water is found in Greenland's fjords and can therefore interact with and melt tidewater glaciers and ice shelves (Straneo et al., 2010; Gladish et al., 2015; Schaffer et al., 2017; Sutherland et al., 2019). The rate at which the ocean melts Greenland's marine boundary can be estimated for floating ice shelves (Wilson et al., 2017; Moyer et al., 2019) but is largely unknown for Greenland's more numerous grounded tidewater glaciers. Observations of the shape of tidewater glacier calving fronts, showing incised undercut chimneys, however provide evidence for rapid submarine melting within upwelling plumes driven by subglacial discharge (Rignot et al., 2015; Fried et al., 2015). Plumes may also enhance submarine melting over the full calving front by driving fjord-wide circulation (Slater et al., 2018; Wagner et al., 2019; Sutherland et al., 2019). There is also a growing body of evidence that submarine melting enhances calving by altering the stress distribution of ice at the calving front (Luckman et al., 2015; Benn et al., 2017a; Ma and Bassis, 2019; How et al., 2019). The emerging picture then is of enhanced submarine melting driving increased calving, leading to retreat and ice sheet mass loss.

In an ideal world then, the ocean boundary conditions supplied to ice sheet models would be submarine melt rates of the marine margin. The ice sheet models would simulate the impact of this melting on calving rate, glacier retreat and ice sheet mass loss. Recent advances mean a handful of ice sheet models have this capability (Bondzio et al., 2016; Aschwanden et al., 2019), but the submarine melt and calving parameterisations employed have yet to be extensively validated, and many other ice sheet models do not have the resolution or technical capability for this approach (Goelzer et al., 2018). As such, we have developed two possible ocean forcing implementations, referred to as the '*retreat implementation*', and the '*submarine melt implementation*' (Fig. 1). The retreat implementation is designed to be implementable by all of the ice sheet models taking part regardless of resolution, model physics or spin-up procedure. In this implementation, retreat of the ice-ocean boundary is

https://doi.org/10.5194/tc-2019-222
Preprint. Discussion started: 26 September 2019


The Cryosphere Discussions

estimated as a linear function of parameterised submarine melting (Slater et al., 2019) and is imposed on an ice sheet model through a time-variable ice mask, an approach first suggested by Cowton et al. (2018). The submarine melt implementation provides ice sheet modeling groups with more freedom by providing fields of subglacial runoff and ocean properties together with a suggested parameterisation for estimating submarine melt from these quantities. The ice sheet modeling group is free to choose how best to force their model with these fields, perhaps by implementing a calving law that depends on submarine melt rate.

Both implementations require a parameterisation for submarine melting. Theoretical considerations suggest that melt rates are controlled primarily by local ocean velocity and ocean thermal forcing, defined as the difference between the in-situ temperature and in-situ freezing point (Gade, 1979; Holland and Jenkins, 1999). Near-ice ocean velocities are thought to be highest inside vigorous plumes resulting from the emergence of buoyant subglacial runoff from the grounding line of the glacier (Mankoff et al., 2016). Submarine melt rate parameterisations (Jenkins, 2011; Xu et al., 2013; Slater et al., 2016) therefore typically include the basic ingredients of subglacial runoff and ocean thermal forcing. For the submarine melt implementation, we follow Rignot et al. (2016) in parameterizing submarine melt rate ($\dot{m}$) as

$$\dot{m} = (3 \times 10^{-4}\, h\, q^{0.39} + 0.15) \times \mathrm{TF}^{1.18} \tag{1}$$

where h is grounding line depth (m), q is the annual mean subglacial runoff normalized by calving front area ($\mathrm{m\,d^{-1}}$) and TF is the ocean thermal forcing defined further below. For the retreat implementation we use a slightly different parameterisation (Slater et al., 2019) in which retreat (dL) is expressed as

$$dL = \kappa \times d(Q^{0.4}\,\mathrm{TF}) \tag{2}$$

where κ is a constant that has been calibrated in Slater et al. (2019) and Q is the mean June-July-August subglacial runoff. This latter parameterisation is slightly simpler than that for submarine melting, but is functionally very similar. We note the slight inconsistency of using annual runoff for the submarine melt implementation and summer runoff for the retreat implementation, but we emphasize that this makes no practical difference since annual and summer runoff are very closely related, even in the future projections when the summer becomes longer (Slater et al., 2019).

The chosen parameterisations require the two basic inputs of future subglacial runoff and ocean thermal forcing, which are estimated from CMIP AOGCMs. While it is hoped that some of the new generation of climate models (CMIP6) will be used in ISMIP6, very few CMIP6 simulations were available at the time of writing, and given the time constraints of the ISMIP6 project, it was decided to focus largely on CMIP5, for which the full ensemble is already available. We therefore here consider 6 CMIP5 AOGCMs (Table 1) that represent a subset of the full CMIP5 ensemble and have been chosen to force ice sheet models in the ISMIP6 effort (Barthel et al., 2019), with a focus on the high greenhouse gas emissions RCP8.5 scenario (Nowicki et al., 2016). Note that each of the CMIP5 AOGCM simulations covers the period 1850-2100, with 1850-2005 considered the historical spin-up period, and the emissions forcing applied from 2006-2100 as defined in the CMIP5 protocol (Taylor et al., 2012). Ice sheet model ocean forcing is delivered for the time period from 1950-2100. The remainder of this methods section describes the calculation of subglacial runoff and ocean thermal forcing from CMIP5 (or CMIP6) output, and the combination of these datasets into ice sheet model ocean forcing in the retreat and submarine melt implementations (Fig. 1).

https://doi.org/10.5194/tc-2019-222
Preprint. Discussion started: 26 September 2019

2.2 Atmosphere

2.2.1 Estimating ice sheet surface runoff using MAR

Since the CMIP5 AOGCMs have a crude representation of ice sheet surface mass balance, the regional climate model MAR (Fettweis et al., 2013) is used to estimate surface runoff by physically downscaling the CMIP5 AOGCM atmospheric fields (Fig. 1). The most recent version of the model, MAR 3.9.6, is run at 15 km resolution with surface mass balance components (including runoff) then statistically downscaled afterwards to 1 km (Franco et al., 2012) to better account for sub-grid topography (Fig. 2a). Each simulation is forced at its boundaries by 6-hourly output from a CMIP5 AOGCM (Table 1), over the period 1950-2100. As will be described in more detail below, the retreat implementation uses June-July-August (JJA) runoff while the submarine melt implementation uses annual runoff. The drainage basins and process of bias correction are the same in each case.

2.2.2 Hydrological drainage basins

Both the retreat and submarine melt implementations use estimates of subglacial runoff per tidewater glacier, which requires a hydrological drainage basin for each glacier (Fig. 1). These basins are delineated based on the hydrological potential (Shreve, 1972):

$$\phi = \rho_w g b + f \rho_i g h \tag{3}$$

where $\rho_w = 1000$ kg m^3 and $\rho_i = 910$ kg m^3 are the densities of freshwater and ice respectively and $g = 9.81$ m^2/s is the gravitational acceleration. Bed topography, b (m), and ice thickness, h (m), come from BedMachinev3 (Morlighem et al., 2017). The variable f represents the flotation fraction (the ratio of subglacial water pressure to ice overburden pressure); here, $f = 1$. By performing flow routing on ϕ (Schwanghart and Scherler, 2014), we identify the area of the ice sheet that drains subglacial water to a given tidewater glacier calving front, thus defining hydrological drainage basins for each tidewater glacier around the ice sheet (Fig. 2b). For simplicity the hydrological drainage basins are assumed to be constant in time. The subglacial runoff for each glacier is then estimated by summing the surface runoff over the hydrological drainage basin for each glacier (Fig. 2b).

2.2.3 Present-day bias correction

The CMIP5 AOGCMs may deviate considerably from the observed present-day climate. They may, for example, be substantially colder than observations, leading to runoff being underestimated in MAR when forced by the AOGCM in question (Fettweis et al., 2013). Since in the ISMIP6 exercise we wish to sample uncertainty in future projections rather than the representation of the present-day, we perform a bias correction of the projected subglacial runoff at each glacier to ensure it agrees with our best estimate of present-day runoff (Fig. 1). This bias correction furthermore ensures a continuous transition from present to future forcing, which is desirable as the ice sheet models have been initialized to the present-day forcing (Goelzer et al., 2018).

https://doi.org/10.5194/tc-2019-222
Preprint. Discussion started: 26 September 2019


The Cryosphere Discussions

Present-day is here defined as the time period 1995-2014. For our best estimate of runoff in the present-day we use a 5.5 km resolution regional climate simulation using RACMO2.3p2, forced at its boundaries by ERA-Interim atmospheric reanalysis (Noël et al., 2018). We ensure that the projected runoff (Q^{PROJ}) agrees with the RACMO runoff (Q^{RACMO}) in the present-day by bias correcting the projected runoff for each glacier (j) as follows:

$$Q_j^{PROJ}(t) \rightarrow Q_j^{PROJ}(t) + \left[Q_j^{RACMO}(\text{1995-2014}) - Q_j^{PROJ}(\text{1995-2014})\right] \quad (4)$$

We thus assume that the bias remains constant in time. An example of this procedure for Helheim Glacier in SE Greenland under MIROC5 in an RCP8.5 scenario is shown in Fig. 2c. In this case the JJA runoff estimated from MAR forced by MIROC5 is decreased by 55 m^3s^{-1} to bring it into agreement with the temporally averaged RACMO2.3p2 output over the period 1995-2014. Bias corrections for the largest glacier by ice flux in each sector and for all models are shown in Fig. S1. We note that it might be thought preferable to have used MAR forced by ERA-Interim for our best estimate of present-day, because it is MAR that is used for the forward projections. We do not however find a significant difference between RACMO and MAR in the present-day (the difference is smaller than the interannual variability) and so we do not believe the use of RACMO causes any inconsistency in methodology.

2.3 Ocean

2.3.1 Defining ocean thermal forcing

The ocean thermal forcing TF entering the parameterisations (Eqs. (1) and (2)) would ideally be that immediately adjacent to the glacier. Waters adjacent to the glacier are known to be a mixture of warm and salty Atlantic waters, cold and fresh polar waters, and even colder and fresher subglacial runoff and submarine meltwater (Straneo et al., 2011; Beaird et al., 2018). Thus the ocean thermal forcing experienced by a glacier is determined by a complex interplay of shelf, fjord and glacier processes (Mortensen et al., 2011; Carroll et al., 2017). The CMIP5 ocean models however have a typical resolution of 20 to 100 km around Greenland, so that even the continental shelves around Greenland are inadequately resolved, and fjords and critical fjord processes are completely absent. By analogy to the atmospheric process already described, one could consider using a regional ocean model to downscale the CMIP5 AOGCMs to the ocean surrounding the ice sheet, but even regional ocean models do not yet represent fjords and fjord processes. Furthermore, we lack simple parameterisations or box models that could represent shelf to fjord to glacier exchange in an efficient fashion. Due to these limitations, we here take a simpler approach to estimating ocean thermal forcing, in which the forcing experienced by the glacier is directly related to far-field ocean properties. As such, we are hard-wiring tidewater glaciers to respond to large-scale ocean changes at the expense of most of the local details that we cannot currently account for. Specifically, we spatially average ocean properties over predefined ocean regions, and use these properties to force all tidewater glaciers in the same region (Fig. 1). For the retreat implementation, the far-field ocean properties are furthermore depth-averaged (details in section 2.4), while for the submarine melt implementation the far-field ocean properties are extrapolated into fjords taking into account bathymetry (details in section 2.5).

https://doi.org/10.5194/tc-2019-222
Preprint. Discussion started: 26 September 2019

2.3.2 Choice of ice-ocean sectors and spatial averaging

The ice sheet and surrounding ocean were divided into 7 ice-ocean sectors (Fig. 3a), over which ocean properties were spatially averaged (Fig. 1). Each sector is hereafter referred to by its acronym (Fig. 3a), where SW is south-west Greenland, CW is central-west Greenland, NW is north-west Greenland, NO is northern Greenland, and similarly for the eastern side of the ice sheet. The sectors, identical to those considered in Slater et al. (2019), were chosen as regions with similar ocean properties largely defined by ocean bathymetry (e.g. Denmark, Fram, Nares Straits) and consistent with the boundaries of commonly used ice sheet drainage basins (e.g. Mouginot et al., 2019) once extended into the ice sheet (see Slater et al. (2019) for a more in depth description). The rather small region in CE Greenland is a transition zone between the warm Atlantic waters in the Irminger basin to the south, and cool Arctic waters in the Nordic Seas to the north and, as such, was split from the respective south and northeast Greenland sectors. Each ice-ocean sector extends to some distance beyond the continental shelf break for two reasons. First, the formulation of the retreat parameterisation required consideration of observed ocean properties from 1960 to present, and the number of available ocean observations increases substantially beyond the shelf break (Slater et al., 2019). Second, the CMIP5 AOGCM ocean components have coarse resolution (e.g. Fig. 3a) and so may not resolve the details of ocean basin to shelf exchange, and may have only a few model points on the continental shelf. By extending the sectors beyond the shelf we are allowing the ice sheet ocean forcing to respond to larger-scale ocean features which may be better resolved by the CMIP5 AOGCMs.

To obtain sector ocean properties, monthly CMIP5 AOGCM outputs of modeled ocean potential temperature (T) and practical salinity (S) are first temporally averaged to annual means (Fig. 3a). Temperature and salinity are then linearly interpolated onto a regular grid with 50 km spatial and 50 m depth resolution (Fig. 3b). Sector ocean properties are finally obtained by taking a simple spatial average over all regular grid points inside a given sector, to give a single temperature and salinity profile for each ice-ocean sector for each year (e.g. Fig. 3c).

2.3.3 Present-day bias correction

As for the subglacial runoff, we bias-correct the ocean properties to ensure consistency with observations in the present-day (Fig. 1). Observations of ocean properties are taken from the Hadley Centre EN4.2.1 dataset (Good et al., 2013), hereafter called EN4. EN4 is a compilation of oceanographic profile data, with a monthly 1900-present gridded product available at 1-degree resolution. We obtain annual profiles per ice-ocean sector from EN4 in the same fashion as for the CMIP5 AOGCM projected profiles. While for subglacial runoff we bias-corrected a single value, here we must bias correct a whole temperature or salinity profile. Rather than applying a different bias correction at each depth level, we apply a single bias correction to the whole profile, based on the observed bias in the 200-500 m depth range. Specifically, we bias-correct ocean temperature (Fig. 3c) as follows

$$T_i^{PROJ}(z,t) \rightarrow T_i^{PROJ}(z,t) + \left[T_i^{EN4}(\text{200-500 m,1995-2014}) - T_i^{PROJ}(\text{200-500 m,1995-2014})\right] \quad (5)$$

Here, $T_i^{PROJ}(z,t)$ is the projected ocean temperature from the CMIP5 AOGCM in ice-ocean sector i at depth z and in the year t. T_i^{EN4}(200-500 m,1995-2014) is the observed ocean temperature in EN4 in sector i, depth-averaged between 200

https://doi.org/10.5194/tc-2019-222
Preprint. Discussion started: 26 September 2019


The Cryosphere Discussions

and 500 m and temporally averaged over the 1995-2014 present-day period. T_i^{PROJ}(200-500 m,1995-2014) is the projected ocean temperature from the CMIP5 AOGCM in sector i, averaged between 200 and 500 m depth and over the present-day period. Salinity is bias-corrected in exactly the same fashion. Since the vertical structure of the ocean can vary in time in the CMIP5 AOGCMs, we felt a depth-varying bias correction could lead to unphysical profiles and that therefore a single-valued correction, centered over the depth range most relevant to tidewater glacier grounding lines (Morlighem et al., 2017), was preferable. As for the runoff, the bias correction is assumed constant in time. The magnitude of these corrections can be significant; for example, for MIROC5 RCP8.5 the temperature bias correction for SE Greenland is 1.4°C (Fig. 3c). Bias corrections for all models and sectors are shown in Fig. S2.

2.4 Retreat implementation

2.4.1 Calculation of ocean thermal forcing

To calculate the thermal forcing that enters the retreat parameterisation in Eq. (2), profiles of ocean temperature and salinity (e.g. Fig. 3c) are first converted to profiles of thermal forcing (Fig. 1). The thermal forcing TF is for the retreat parameterisation defined as the elevation of the potential ocean temperature T above its local freezing point T_f

$$\mathrm{TF}_i(z,t) = T_i(z,t) - T_{f,i}(z,t) = T_i(z,t) - [\lambda_1 S_i(z,t) + \lambda_2 + \lambda_3 z] \tag{6}$$

where in the second equality we have employed a linearized expression for the local freezing point in terms of the practical salinity S and depth z, and the constants take values $\lambda_1 = -5.73\times10^{-2}$, $\lambda_2 = 8.32\times10^{-2}$, and $\lambda_3 = 7.61\times10^{-4}$ m^{-1} (Jenkins, 2011). As before, i indexes the ice-ocean sector.

In-keeping with the simple philosophy of the retreat parameterisation, the profiles of thermal forcing $\mathrm{TF}_i(z,t)$ are finally depth-averaged between 200 and 500 m depth, this being the depth range most relevant to tidewater glacier grounding lines in Greenland (Morlighem et al., 2017). The final thermal forcing entering Eq. (2) in the retreat implementation is therefore a single value per ice-ocean sector, per year, for each CMIP5 model considered (Table 1).

2.4.2 Glacier-by-glacier projection of retreat

For each CMIP5 AOGCM, we first estimate retreat for each of the 191 individual tidewater glaciers considered in Slater et al. (2019) by employing Eq. (2) with the summer subglacial runoff Q per glacier (section 2.2) and ocean thermal forcing TF per sector (section 2.3). Specifically, for each glacier j from 1 to 191 we form the time series $Q_j^{0.4}\,\mathrm{TF}_{i(j)}$ where $i(j)$ is the ice-ocean sector i from 1 to 7 in which the glacier j is situated (Fig. 4a). Since this time series has high interannual variability, and since for ISMIP6 we are most interested in the multi-decadal sea level contribution, the time series is smoothed using a 20-year centered moving average (Fig. 4a). Lastly, in the CMIP6 and ISMIP6 frameworks (Nowicki et al., 2016; Eyring et al., 2016) the projections begin in 2015, and we therefore project retreat relative to 2014. Thus for each glacier j, projected retreat $dL_j(t)$ is given by

$$dL_j(t) = \kappa \times \left[Q_j^{0.4}\,\mathrm{TF}_{i(j)}(t) - Q_j^{0.4}\,\mathrm{TF}_{i(j)}(t=2014)\right] \tag{7}$$

https://doi.org/10.5194/tc-2019-222
Preprint. Discussion started: 26 September 2019

where both terms on the right-hand side refer to the smoothed time series. As described in Slater et al. (2019), the coefficient κ is sampled from a distribution that was obtained by calibrating the parameterisation to observed tidewater glacier retreat over the full ice sheet over the past 60 years. The distribution has a median value $\kappa = -0.17$ and lower and upper quartiles $\kappa = -0.37$ and $\kappa = -0.06$ respectively. We generate 10^4 possible future retreat trajectories for each glacier (Fig. 4b) by sampling 10^4 values of κ from its distribution.

2.4.3 Averaging retreat per ice-ocean sector

Due to limitations of the retreat parameterisation - principally its lack of ability to capture individual glacier effects related to bed topography - it is most appropriate to apply retreat averaged over a population of glaciers rather than on an individual glacier basis (Slater et al., 2019). From the ice sheet model perspective, this is also preferable because the state of the ice sheet may differ significantly from the observed ice sheet (Goelzer et al., 2018). Thus identifying individual glaciers in a given ice sheet model is not trivial, and therefore applying retreat to individual glaciers is also difficult. An obvious solution is to impose a given retreat over a predefined geographical region (or ice-ocean sector), which means averaging retreat over a population of glaciers.

A potential issue is that under the retreat parameterisation (Eq. (2)), glaciers with large hydrological catchments (typically glaciers such as Jakobshavn Isbrae or Helheim) undergo large changes in subglacial runoff and therefore have large projected retreat relative to smaller glaciers. This is considered an important feature of the retreat parameterisation (Slater et al., 2019). Each ice-ocean sector (Fig. 3a) typically has a small number of large glaciers and a large number of small glaciers, such that taking a simple mean of the projected retreat over the glaciers in a sector will result in a trajectory that is much closer to that of the small glaciers than the large glaciers. This is problematic because the primary objective of ISMIP6 is sea level contribution, and for Greenland this is dominated by the largest glaciers (Enderlin et al., 2014). To address this problem, we take an ice flux-weighted mean over glaciers in a sector (Fig. 1). Specifically, we define the retreat for each sector i as

$$dL_i(t) = \sum_{j \in i} f_j \, dL_j(t) \, / \sum_{j \in i} f_j \tag{8}$$

where f_j is the 2000-2010 mean observed ice flux (Enderlin et al., 2014; King et al., 2018) and the sum runs over all glaciers j in ice-ocean sector i. This ensures that the largest glaciers are treated as the most important when generating a retreat projection per sector. Since we have 10^4 retreat trajectories for each glacier (Fig. 4b), this procedure produces an ensemble of 10^4 ice flux-weighted retreat trajectories for each ice-ocean sector. As expected, the median retreat of this ice flux-weighted ensemble is larger than the median retreat that would have been obtained by taking a simple mean over glaciers in a sector (Fig. 4c).

2.4.4 Low, medium and high scenarios

Given the large uncertainty associated with tidewater glacier response to climate forcing, and the need to quantify uncertainties on future sea level contributions, it is desirable to provide a range of projected retreat that brackets the uncertainty associated with the retreat implementation. Thus for each CMIP5 AOGCM we identify a low, medium and high retreat scenario (Fig. 1). From the ensemble of 10^4 ice flux-weighted retreat trajectories for each ice-ocean sector, we define the medium retreat scenario

https://doi.org/10.5194/tc-2019-222
Preprint. Discussion started: 26 September 2019

as the trajectory with the median retreat at 2100, and the low and high retreat scenarios as the trajectories with the 25th and 75th percentile retreats at 2100 (Fig. 4c).

2.5 Submarine melt implementation

2.5.1 Extrapolation of ocean properties into fjords

In the submarine melt implementation, we account for the effects of fjord bathymetry and grounding line depth on the thermal forcing experienced by the glacier (Fig. 1). This is achieved by extrapolating the ocean property profiles (e.g. Fig. 3c) into fjords and below the present-day ice sheet by taking into account ocean bathymetry and subglacial topography in the same manner as Morlighem et al. (2019), based on the BedMachinev3 topography (Morlighem et al., 2017). Specifically, for each location in a fjord and beneath the present-day ice sheet, the deepest point that is openly connected to the wider ocean is determined; this depth is hereafter termed the effective depth. Water shallower than the effective depth is assumed to communicate directly with the open ocean and is therefore assigned the temperature and salinity profile for the sector in question. Water deeper than the effective depth is not in direct communication with the open ocean, due to the blocking effect of bathymetry, and is therefore uniformly assigned a temperature and salinity equal to that at the effective depth.

An illustrative example is given for Sverdrup Glacier, NW Greenland, and the adjacent ocean (Fig. 5). The fjord mouth has full-depth open communication with the ocean and is therefore assigned unmodified ocean properties for the NW sector (yellow profiles in Figs. 5b-d). The bed topography at a point beneath the present day ice sheet reaches 600 m below sea level, but, assuming the glacier had retreated past this point, would be separated from the open ocean by a sill at ∼350 m depth (Figs. 5a and b). By our extrapolation, this 600 m deep region is isolated from the warmest and saltiest water on the continental shelf. Thus the ocean properties in this deep region (red profiles in Figs. 5b-d) diverge from those at the fjord mouth below the height of the sill. This procedure is repeated for all fjords around the ice sheet, including below the present-day ice sheet, so that ocean conditions at calving fronts will be available to ice sheet models after calving fronts have retreated.

2.5.2 Calculation of ocean thermal forcing

In line with the more complex nature of the submarine melt implementation relative to the retreat implementation, we use full, non-linear TEOS-10 routines (McDougall and Barker, 2011) to convert ocean property profiles to ocean thermal forcing profiles (Figs. 1 and 5d). Specifically, the CMIP5 quantities of depth, practical salinity and potential temperature are converted to pressure, absolute salinity and in-situ temperature using the 'gsw_p_from_z', 'gsw_SA_from_SP' and 'gsw_t_from_pt0' routines respectively. A full three-dimensional, time-varying thermal forcing field $\mathrm{TF}(x,y,z,t)$ is then obtained as

$$\mathrm{TF}(x,y,z,t) = T(x,y,z,t) - T_f(x,y,z,t) \tag{9}$$

Where T is the in-situ temperature and T_f is the in-situ freezing point that depends on pressure and absolute salinity as defined by the 'gsw_t_freezing' routine. Lastly, we collapse the three-dimensional thermal forcing field to two-dimensions by considering only the value at the ocean bottom, so that the final thermal forcing field TF is defined at annual resolution on a 1

https://doi.org/10.5194/tc-2019-222
Preprint. Discussion started: 26 September 2019

km x-y grid covering Greenland (Fig. 6a). The motivation for using the ocean bottom value is that this is the thermal forcing experienced by the grounding line of a glacier if its calving front was located in the grid cell in question.

2.5.3 Assignation of runoff to drainage basins

The treatment of subglacial runoff is initially the same as for the retreat parameterisation. Once the time series of bias-corrected subglacial runoff has been obtained for each marine-terminating glacier (section 2.2), this runoff is distributed onto a 1 km x-y grid by assigning the total runoff for each hydrological basin (Fig. 2b) to every grid point lying inside the basin (Figs. 1 and 6b). In this way, as a calving front retreats over the x-y grid, the calving front submarine melt rate may be obtained by sampling the ocean thermal forcing and subglacial runoff from the grid point at which the calving front is currently located. We assume that the hydrological drainage basins remain fixed in time at their present-day extent. Extending the runoff field beyond the present-day ice sheet is however desirable to allow for potential calving front advance in the simulations, or to accommodate models whose initial ice extent is larger than observations. We choose to extrapolate subglacial runoff values beyond the present-day ice sheet by three 1 km grid cells using an iterative buffering approach. First, we sort the drainage basins by area from largest to smallest. For each iteration, we buffer runoff values by one 1 km grid cell around each basin, starting with the largest basin and ending with the smallest basin. We fill only empty grid cells such that if grid cell has already been populated by a runoff value from a larger basin, we do not overwrite that value. In this way, grid cells that are adjacent to two drainage basins are filled with runoff values from the larger basin. After the third iteration, we are left with a field of annual cumulative basin runoff values that have been extrapolated by three 1 km grid cells beyond the present-day ice sheet extent.

The submarine melt parameterization Eq. (1) takes as input the subglacial runoff normalized by the submerged area of the calving front for each glacier. The submerged area will change over the course of the ice sheet model simulations as the termini retreat through fjords of various depths and widths. Since dynamically calculating the submerged area is difficult within an ice sheet model, we assume that the submerged area of each terminus remains constant at present-day values (c.f. Morlighem et al., 2019). The present-day submerged surface area is calculated based on present-day calving front position and bed topography as defined by BedMachinev3 (Morlighem et al., 2017). Due to poor bed topography in some regions, which typically means unrealistically shallow topography in the region of a calving front, we impose a minimum submerged surface area of 0.2 km^2, equivalent to a glacier of width 2 km and grounding line depth 100 m.

2.5.4 Application of submarine melt parameterisation

Armed with both ocean thermal forcing and subglacial runoff fields defined at annual resolution on 1 km grids, and with the submarine melt rate parameterisation Eq. (1), submarine melt rates may be estimated for the time period 1950-2100 and for each CMIP5 model (Fig. 1 and Table 1). While this defines a submarine melt rate on every grid cell where both ocean thermal forcing and runoff are defined (Fig. 6c), the intention is that the ice sheet model applies this submarine melt rate only when the model has a calving front within this grid cell. In this way, the ice sheet models may apply a time-varying submarine melt rate to calving fronts around the ice sheet as these calving fronts retreat over the coming century.

https://doi.org/10.5194/tc-2019-222
Preprint. Discussion started: 26 September 2019

3 Results

We here present the Greenland Ice Sheet ocean forcing arising from the choices and steps made in section 2. The intention is to highlight temporal evolution of the forcing, together with spatial and model-to-model variability, as these factors will drive variability in sea level projections once implemented in an ice sheet model. The results are discussed with the same structure as section 2 and Fig. 1.

3.1 Future atmosphere

For both implementations, projected subglacial runoff is prescribed for each tidewater glacier and hydrological drainage basin. We visualize variability in runoff by considering runoff for the largest glacier by ice flux in each sector (Table S1), as these glaciers are likely to contribute the most to sea level over the coming century. These glaciers are Helheim (SE), Kangiata Nunata Sermia (SW), Kangerdlugssuaq (CE), Jakobshavn (CW), Daugaard-Jensen (NE), Kong Oscar (NW) and Humboldt (NO); note that in the retreat implementation, glaciers having permanent ice shelves have been excluded. Runoff shows high interannual variability and so we also plot and discuss smoothed curves.

In the MIROC5 RCP8.5 simulation, all glaciers show a significant increase in runoff by 2100, with most of the increase occurring after 2050 (Fig. 7a). Jakobshavn (CW) and Humboldt (NO) show the largest absolute increase in runoff, with Daugaard-Jensen (NE) and Kong Oscar (NW) having the smallest runoff anomaly (Fig. 7a). Since the absolute runoff enters the retreat parameterisation Eq. (2), Jakobshavn and Humboldt may therefore have higher projected retreat than Daugaard-Jensen and Kong Oscar. Whether this feeds through into the sector retreat projections depends also on the ocean thermal forcing and the projected retreat of the other glaciers in the sector.

A different picture of spatial variability however emerges when considering the relative runoff anomaly (Fig. 7b). In this case it is Kong Oscar (NW) that stands out, with JJA runoff in 2100 a factor of 8 larger than during the 1995-2014 baseline period. Kangiata Nunata Sermia (SW) also experiences a large relative increase in runoff, while Daugaard-Jensen (NE) sees the smallest, amount to only a factor 2.5 larger than in 1995-2014. Equivalent plots for all other CMIP5 AOGCMs are shown in Figs. S3 and S4, but show very similar spatial variability to MIROC5.

Lastly, we consider model-to-model variability in projected runoff by averaging over the largest glacier in each sector (Fig. 7c). The only RCP2.6 scenario considered shows a moderate increase in runoff until 2050 before a return to present-day values by 2100 (Fig. 7c). All RCP8.5 simulations exhibit a similar temporal evolution and show a significant increase in runoff by 2100. Runoff in HadGEM2-ES, IPSL-CM5A-MR and MIROC5 is high and very similar in 2100, NorESM1-M and ACCESS1-3 have medium runoff and CSIRO-Mk3-6-0 has the lowest runoff. This model-to-model variability is as would be expected from the ISMIP6 CMIP5 model evaluation exercise (Barthel et al., 2019). The multi-model spread in runoff anomaly at 2100 is $\sim$850 $m^3 s^{-1}$; around 50% of the multi-model mean of $\sim$1650 $m^3 s^{-1}$.

https://doi.org/10.5194/tc-2019-222
Preprint. Discussion started: 26 September 2019

3.2 Future ocean

We present ocean results based on the sector-averaged, depth-averaged time series derived for the retreat implementation (section 2.4.1). While the submarine melt implementation differs by retaining depth variability and through the extrapolation of properties into fjords, the depth-averaged values from the retreat implementation remain a reliable indicator of what the ocean does.

There is significant regional variability in projected ocean warming in the MIROC5 RCP8.5 simulation (Fig. 8a). The NE sector stands out with a thermal forcing increase of nearly 5°C, while all other sectors exhibit an increase of between 1 and 3°C. Ocean warming in the NE sector amounts to an increase of 150% in thermal forcing relative to the 1995-2014 baseline period (Fig. 8b). The SE and SW sectors see the smallest relative increase amounting to only ∼20%. We do note however that regional ocean warming differs substantially across CMIP5 AOGCMs (Yin et al., 2011; Barthel et al., 2019, Figs. S5 and S6). The NE sector sees the most warming in MIROC5, HadGEM2-ES and IPSL-CM5A-MR, but the CW and NW regions see equivalent or greater warming in the other three models. It is also interesting to note that the relative increase in runoff (Fig. 7b) is much larger than the relative increase in ocean thermal forcing (Fig. 8b).

We consider ocean warming at the ice sheet scale by taking a mean over the 7 sectors for each CMIP5 AOGCM (Fig. 8c). For MIROC5 RCP2.6, there is moderate warming of nearly half a degree which persists until the end of the century. This is mostly driven by significant warming in the CW and NW sectors (Fig. S5a) that exceeds warming in these sectors in some of the RCP8.5 simulations (Figs. S6d and S6f). Given the large inter-model variability in ocean warming, this warming feature is likely to be specific to MIROC5 rather than being more broadly representative of RCP2.6 simulations. Among the RCP8.5 simulations, CSIRO-Mk3-6-0 is overall the warmest by 2100 with nearly 3°C of warming, while HadGEM2-ES and NorESM1-M are the coldest with 2°C of warming. The multi-model spread in thermal forcing anomaly in 2100 is 0.9°C, around 35% of the multi-model mean of ∼2.4°C.

3.3 Retreat implementation forcing

Projected sector retreat combines the runoff anomaly per glacier (section 3.1), the thermal forcing anomaly per sector (section 3.2), and the ice flux of all glaciers in the sector (section 2.4.3). Thus sector-to-sector variability in projected retreat arises due to both variability in regional climate, and differences in the population of glaciers in each sector.

For the MIROC5 RCP8.5 simulation, the SW sector has the largest retreat (Fig. 9a) because it has a small number of glaciers (Table S1) each experiencing a large increase in subglacial runoff (Figs. 7a-b). The projected retreat for the CW sector is also high (Fig. 9a), partly due to large projected retreat for Jakobshavn, which then dominates the sector-average retreat, because it alone accounts for around half of the present-day ice flux in the CW sector (Table S1). Projected retreat is smallest for the NW and NO sectors (Fig. 9a) because these sectors comprise a large population of smaller glaciers (Table S1) and experience the least absolute increase in subglacial runoff (Fig. 7a). Figure S7 shows equivalents plots to Fig. 9a for all other CMIP5 AOGCMs - the spatial patterns of retreat are similar in almost all models with large projected retreat for SW and CW and

https://doi.org/10.5194/tc-2019-222
Preprint. Discussion started: 26 September 2019

smaller retreat for NW and NO. Note that Fig. 9a shows only the medium retreat case for each sector; low and high projections are plotted in Fig. S8.

To provide an ice sheet-wide view of retreat per CMIP5 AOGCM, we combine the sector-by-sector projections (e.g. Fig. 9a) into an ice sheet projection by weighting according to the present-day ice flux (Table S1). The resulting projections (Fig. 9b) are not used to force the ice sheet models (the ice sheet models are forced by the sector-by-sector projections), but they do illustrate multi-model variability in projected retreat. The RCP2.6 simulation considered shows moderate retreat of ∼2 km until 2050 and then a stabilization of terminus positions (Fig. 9b). The retreat is largely driven by significant ocean warming in the CW and NW sectors (Figs. S5a and S7a).

The RCP8.5 projections show ∼15 km of retreat by 2100. The retreat rate generally increases throughout the century, so that ∼4 km of retreat occurs before 2050 and ∼11 km between 2050 and 2100. The multi-model spread in retreat by 2100 is only 2 km, or 15% of the multi-model mean. The largest retreat is projected using CSIRO-Mk3-6-0 and the least using HadGEM2-ES, although all models are similar. In contrast, the spread in projections resulting from the low and high retreat cases for a given model is generally large. For the MIROC5 RCP8.5 projections, the difference between the low and high retreat cases at 2100 is 14 km, much larger than the multi-model spread (Fig. 9b). The same is true for the low and high cases in all other RCP8.5 models (not shown).

3.4 Submarine melt implementation forcing

Projections of submarine melt rates are obtained by combining ocean thermal forcing, runoff accumulated over each glacier's subglacial drainage basin, and a calving front submerged area (Eq. (1)). To illustrate the results, we show melt rates for the glacier with the largest ice flux in each region (Fig. 10; Table S1). These projections do not take into account the motion of glacier termini and, thus, isolate the change in melt rates due solely to changes in future ocean and atmospheric forcing.

Submarine melt rates increase over the projection timespan (2015-2100) under all RCP8.5 scenarios for all 7 glaciers, although the magnitude and timing of the increase varies by location and by CMIP5 model (Fig. 10). At Humboldt Glacier in the north, little increase is seen until 2060, after which the models diverge with a range of 0.5 to 2 $\mathrm{m\,d^{-1}}$ projected melt rate in 2100 (Fig. 10b). In the NW, NE and central regions (Jakobshavn, Kangerdlussuaq, Kong Oscar, and Daugaard-Jensen), melt rates increase soon after 2015 and are up to 5 times larger in 2100 relative to the 1995-2014 baseline period (Figs. 10c-f). In the south (Kangiata Nunata Sermia and Helheim), melt rates double or triple by 2100 under RCP8.5 (Figs. 10g-h). There is significant spread in projected melt rates in 2100 for the RCP8.5 scenarios, typically amounting to 25-50% of the multi-model mean, but substantially more for Humboldt Glacier. When considering a mean over the 7 glaciers, the multi-model spread under RCP8.5 is much smaller than at individual glaciers, with the mean melt rate increasing from ∼2 $\mathrm{m\,d^{-1}}$ in the present-day to ∼6 $\mathrm{m\,d^{-1}}$ in 2100 (Fig. 10a). Under the RCP2.6 scenario, melt rates show only moderate increases until around 2050, followed by stabilization or decrease (Fig. 10). Projected RCP2.6 melt rates in 2100 are lower than the present day for Kangiata Nunata Sermia and Helheim (Figs. 10g-h). In general, RCP2.6 melt rates do not depart significantly from RCP8.5 melt rates until around 2050.

https://doi.org/10.5194/tc-2019-222
Preprint. Discussion started: 26 September 2019

A similar picture emerges when a larger population of 125 glaciers is considered. Figure 11 shows histograms of the relative increase in submarine melt rate between a twenty year period the end of the century (2081-2100) and the present-day (1995-2014) under all 6 of the RCP8.5 models considered (thus Fig. 11a has a total count of 58 x 6 = 348). In SE and SW Greenland, melt rates increase by at most 170%. These regions already experience a warm ocean and atmosphere in the present-day and so large increases in absolute melt rate (Figs. 10g-h) appear as smaller relative increases in submarine melting. Moving north, CE, CW and NW Greenland experience increases up to ∼400% while the NE and NO sectors have the largest relative increases in melting, reaching over 1000%. These northerly regions have a particularly cold ocean in the present-day and therefore currently experience very little submarine melting (e.g. Fig. 10b). Thus any increase in absolute melt rate can constitute a very large relative increase.

The spread in relative melt rate increase within regions (Fig. 11) arises from a number of factors. The glaciers in each region have diverse grounding line depths, submerged in fjords with differing sill depths. Thus glaciers with deep grounding lines that are directly exposed to the ocean are responding to different water masses than glaciers that are grounded in shallow water or protected from the ocean by shallow sills. If these water masses evolve differently over the coming century, then adjacent glaciers may experience very different ocean forcing even within the same CMIP5 AOGCM. A second source of variability is that from the 6 CMIP5 AOGCMs themselves, which can differ substantially on the evolution of ocean temperature within a given sector (Fig. S6).

4 Discussion

4.1 Retreat and submarine melt implementations

This paper has presented the ocean forcing strategy for ice sheet models taking part in ISMIP6. Driven by a need to compromise between process understanding and AOGCM and ice sheet model limitations, we have proposed two approaches termed the retreat implementation and submarine melt implementation (Fig. 1). Under the retreat implementation, retreat is prescribed for each of 7 ice sheet-ocean sectors (Fig. 9a) and imposed on an ice sheet model by a time-dependent ice-sheet mask. Under the submarine melt implementation, fields of subglacial runoff, ocean thermal forcing and a submarine melt parameterisation are provided, allowing an ice sheet model to estimate submarine melt rate for the current position of the calving front (Figs. 10 and 11), and apply this to the ice sheet model as they see fit. Each implementation has distinct advantages and disadvantages, and in fact, it will be very interesting to contrast modeled ice sheet response between the two implementations.

The retreat implementation has the advantage of being accessible to all ISMIP6 ice sheet models, and has been empirically validated by tuning to match observed glacier retreat over the past 60 years (Slater et al., 2019). In addition, it replaces the need for a representation of calving, the parameterisation of which remains a large source of uncertainty (Benn et al., 2017b). On the other hand, the retreat implementation does parameterize terminus position in a rather constraining manner; it does not allow for modeled ice dynamics to influence the terminus position, and it takes no account of bed topography, which is known to be an important factor in determining the response of an individual glacier to an ocean perturbation (e.g. Catania et al., 2018).

https://doi.org/10.5194/tc-2019-222
Preprint. Discussion started: 26 September 2019

While the use of a retreat averaged over a population of glaciers in a region does ameliorate these issues (Slater et al., 2019), it would be ideal to instead resolve such glacier-specific dynamics, which motivates the second proposed implementation.

The submarine melt implementation places less constraints on the interaction between the ocean and ice sheet by specifying only the submarine melt rate (or more precisely, the subglacial runoff, ocean temperature and a parameterisation to combine these quantities to estimate submarine melt rate). The representation of calving, and its possible coupling to submarine melting, is left to the ice sheet model. This implementation has the advantage that the important interactions between submarine melting, calving, ice dynamics and bed topography can be resolved by the model (e.g. Morlighem et al., 2019). The disadvantages are that there is large uncertainty in the submarine melt rates obtained from the parameterisation and we still lack a good understanding of, and parameterisation for, calving. Furthermore, the submarine melt implementation may be considerably more computationally expensive and technically challenging to implement than the retreat implementation.

4.2 Variability in projections

The CMIP5 models considered (Table 1) display a considerable spread in future atmosphere and ocean projections. Under an RCP8.5 scenario, the subglacial runoff anomaly averaged over the largest glacier in each sector in 2100 ranges from 1150 m^3s^{-1} in CSIRO-Mk3-6-0 to nearly 2000 m^3s^{-1} in HadGEM2-ES (Fig. 7c). Relative to the 1995-2014 mean of 440 m^3s^{-1}, this represents an increase by a factor 2.5-4.5. In contrast, the only RCP2.6 model considered has almost no runoff anomaly by the end of the century but does show elevated runoff for much of the coming century (Fig. 7c). Similarly, for the ocean and under an RCP8.5 scenario, the thermal forcing anomaly by the end of the century varies from 1.9°C for HadGEM2-ES to 2.8°C for CSIRO-Mk3-6-0 over a 1995-2014 baseline of 4.6°C, an increase by a factor 0.4-0.6 (Fig. 8c). Regional variability exhibits a much larger spread. Under RCP2.6, there is warming of $\sim$0.3°C by the end of the century (Fig. 8c). It should be borne in mind that the 6 CMIP5 models we have analysed in this paper are a selected subset of the larger CMIP5 ensemble (Barthel et al., 2019), which exhibits an even greater spread in future projections.

While the projected increase in subglacial runoff is much higher than for ocean thermal forcing for all models under an RCP8.5 scenario (Figs. 7 and 8), both forcings contribute significantly to the retreat and submarine melt rate projections due to the form of the retreat and submarine melt parameterisations (Eqs. (1) and (2)). The subglacial runoff Q appears sub-linearly in these parameterisations, while the thermal forcing TF appears approximately linearly, so that the impact of increasing thermal forcing is larger than the impact of increasing runoff by an equivalent amount.

There also appears to be some compensation occurring between atmosphere and ocean in the 6 AOGCMs we have considered. The model that has the most ocean warming (CSIRO-Mk3-6-0) has the least runoff increase, and the model that has the least ocean warming (HadGEM2-ES) has the most runoff increase (Figs. 7 and 8). Due to the form of the retreat and submarine melt parameterisations (Eqs. (1) and (2)), the atmosphere and ocean projections can compensate each other, reducing the multi-model spread in the retreat and submarine melt projections (Figs. 9b and 10). Coupled with the large uncertainty on the linear coefficient κ appearing in the retreat parameterisation (Slater et al., 2019), the spread in projected retreat due to the low and high retreat cases (section 2.4.4) is therefore much larger than the spread in projected retreat due to AOGCM selection (Fig. 9b). It can therefore be expected that the spread in sea level projections arising from the use of the retreat implemen-

https://doi.org/10.5194/tc-2019-222
Preprint. Discussion started: 26 September 2019

tation will be larger when comparing low and high retreat scenarios than when comparing retreat forced by different CMIP5 AOGCMs.

Examination of the projected submarine melt rates (Fig. 10) also suggests the possibility for sector-by-sector compensation. Explicitly, there is no individual CMIP5 model that gives high melt rates in every single sector or at every single glacier; rather a model that gives high melt rates in a certain sector often gives lower melt rates in another sector. As a result, taking a mean of the projected RCP8.5 melt rates over 7 large glaciers gives trajectories that lie within a narrow envelope (Fig. 10a). This sector-by-sector compensation may act to reduce differences in projected sea level contribution between different CMIP5 AOGCMs.

It should be said that while projected retreat and submarine melt may look similar in all AOGCMs at an ice sheet scale, the same is not true of individual sectors or glaciers, where the AOCGMs can differ quite substantially (Figs. 10, S4 and S6). Furthermore, the dynamic sea level contribution is not directly related to the magnitude of retreat or submarine melt rate. For example, although the SW sector has the largest projected retreat, it contains relatively few tidewater glaciers and these glaciers currently account for <4% of Greenland's ice discharge (Table S1). It is therefore unlikely to be a major source of dynamic sea level contribution in the future. In contrast, the NW region has the smallest projected retreat, but has a large number of tidewater glaciers that currently account for ∼20% of Greenland's ice flux (Table S1), and is therefore much more likely to be a significant dynamic contributor to sea level. Within the submarine melt implementation there is also the possibility for non-linear or threshold response of glaciers to submarine melting, where small changes in forcing may result in large excursions in terminus position and mass loss (Morlighem et al., 2019). Once again therefore, multi-model variability the ice sheet sea level contribution may differ from multi-model variability in the forcings described in this paper.

4.3 Missing processes and priorities for future improvement

Due to the complexity and timescale of the exercise we have had to make a number of simplifications of complex processes in order to deliver the ocean forcing to the ice sheet modeling groups. One key simplification is our treatment of the ocean thermal forcing experienced by tidewater glaciers. Since the CMIP5 AOGCMs do not resolve Greenland's fjords, we have had to bridge the gap between the continental shelf and calving fronts. In the retreat parameterisation, the ocean thermal forcing applied to glaciers is a spatially- and depth-averaged value from the continental shelf. Thus we have neglected spatial gradients in ocean temperatures within the chosen sectors (Slater et al., 2019), the fjord processes responsible for transporting and transforming ocean waters between the shelf and calving front (Motyka et al., 2003; Straneo et al., 2010; Mortensen et al., 2011; Jackson et al., 2014; Gladish et al., 2015), and the diverse grounding line and sill depths of glaciers and fjords in Greenland (Morlighem et al., 2017). We do note that the retreat parameterisation Eq. (2) was tuned based on observations from 1960 to present using the same definition of ocean thermal forcing and so, to some extent, all of these processes will have fed into the empirical tuning. This definition of ocean thermal forcing nevertheless neglects much of the individuality of glacier-fjord systems, essentially linking groups of glaciers to large-scale ocean changes only.

In the submarine melt implementation, the effect of sills and grounding line depth is taken into account by retaining the depth-variability of ocean conditions and extrapolating these properties into fjords based on the bathymetry. Certainly, the

https://doi.org/10.5194/tc-2019-222
Preprint. Discussion started: 26 September 2019

presence of sills is known to modify fjord water properties substantially by blocking access of dense waters to the calving front (Gladish et al., 2015), but this extrapolation remains a simplification because periodic dense inflows over sills have been observed in Greenland (Mortensen et al., 2011). Therefore both the retreat and submarine melt implementations would be improved with methods to quantify water mass transformation between the shelf and calving fronts; such methods might take the form of very high-resolution regional ocean modeling or, perhaps more practically for efforts such as ISMIP6, simple parameterisations or fjord box models.

Both implementations also assume that submarine melting is the primary climate forcing experienced by the calving fronts of tidewater glaciers. This assumption derives from the literature consensus on the important role played by submarine melting in the recent retreat of tidewater glaciers in Greenland (Holland et al., 2008; Straneo and Heimbach, 2013; Fried et al., 2015; Cowton et al., 2018), yet other processes may also play a role. In particular, the buttressing provided to glaciers by ice mélange may be sufficient to suppress calving (Amundson et al., 2010; Robel, 2017), has been implicated in rapid glacier retreat (Christoffersen et al., 2012; Moon et al., 2015; Bevan et al., 2019), and is found to be more influential than submarine melt in some models (Krug et al., 2015; Todd et al., 2018). Future ice sheet ocean forcing efforts might therefore look to quantify the impact of ice mélange buttressing.

Once submarine melting is assumed to be the primary ocean forcing, it must be parameterised, as has been done in Eqs. (1) and (2) for the submarine melt and retreat implementations respectively. The form of both parameterisations derives from the physics of plumes, which are relatively well understood from theory and laboratory and observational work (Morton et al., 1956; Jenkins, 2011; Jackson et al., 2017). Observations of submarine melting with which to constrain key constants in melt parameterisations are however severely lacking; our first direct observations of submarine melting were obtained very recently in Alaska (Sutherland et al., 2019) and suggested we may currently be underestimating submarine melt rates, especially outside of plumes. For the retreat implementation, uncertainty in melt parameterisations is less of an issue because the parameterisation assumes proportionality between glacier retreat and submarine melt rate, and since glacier retreat is easily observable, we have good observations to tune the linear coefficient κ (Slater et al., 2019). This is not the case for the submarine melt implementation, though ice sheet models typically do a spin-up simulation in which they tune their model to try to match present-day ice sheet extent, which may go some way to reducing their sensitivity to uncertainty in the melt parameterisation. It is clear however that observations of submarine melting, and further work building on Sutherland et al. (2019), would be valuable for reducing uncertainties on sea level contribution in efforts beyond ISMIP6.

5 Summary

The Ice Sheet Model Intercomparison Project for CMIP6 (ISMIP6) constitutes the primary community effort to produce ice sheet sea level projections for the next Intergovernmental Panel on Climate Change Assessment Report (IPCC AR6). ISMIP6 is the first effort to develop a multi-model ensemble of Greenland ice sheet models forced by ocean boundary conditions derived from CMIP AOGCMs. Such a strategy is demanding to design due to the evolving nature of our process understanding and ice sheet model technical capabilities. With these challenges in mind, we have proposed two ocean forcing strategies, called the

https://doi.org/10.5194/tc-2019-222
Preprint. Discussion started: 26 September 2019

'retreat implementation' and the 'submarine melt implementation'. By combining these strategies with projected climate from selected CMIP AOGCMs, we have derived ocean boundary conditions for Greenland Ice Sheet models to run 21st century projections.

In the retreat implementation, retreat is projected using a process-motivated but empirically-calibrated parameterisation that relates tidewater glacier terminus position to estimated submarine melt rate (Slater et al., 2019). Retreat is projected for each individual tidewater glacier, but for simplicity is applied to the ice sheet homogeneously within each of 7 sectors. Under a high greenhouse gas emissions RCP8.5 scenario, projected retreat that will be applied to the ice sheet models amounts to around 15 km by 2100 with a range of 10-25 km in low and high scenarios. Under a low emissions RCP2.6 scenario, retreat of only $\sim$1 km will be prescribed. In the submarine melt implementation, fields of subglacial discharge and ocean thermal forcing covering Greenland are provided, together with a recommended parameterisation that may be used to estimate submarine melt rate wherever a calving front is located. Under RCP8.5, projected melt rates in 2100 are a factor $\sim$3 higher than the present-day, but remain relatively constant under RCP2.6. The sea level contributions resulting from these two implementations will be determined by the modeled dynamic response to these forcings.

The proposed implementations are driven by process understanding but are also pragmatic and have necessarily neglected certain processes or made use of poorly-constrained parameterisations. Foremost amongst these are fjord processes and the transformation of ocean waters between the continental shelf and glacier calving front, and the parameterisation of submarine melting. These issues are to some extent ameliorated through tuning, both in the described implementation and at the level of the ice sheet model. Nevertheless, research constraining submarine melt parameterisations and calving laws, and developing simple methods for quantifying fjord transformation of ocean waters, should remain a high priority for reducing uncertainty on the future sea level contribution of the Greenland Ice Sheet.

https://doi.org/10.5194/tc-2019-222
Preprint. Discussion started: 26 September 2019

MODEL	SCENARIO
MIROC5	RCP2.6 & RCP8.5
NorESM1-M	RCP8.5
HadGEM2-ES	RCP8.5
CSIRO-Mk3-6-0	RCP8.5
IPSL-CM5A-MR	RCP8.5
ACCESS1-3	RCP8.5

Table 1. CMIP5 AOGCMs and scenarios considered.

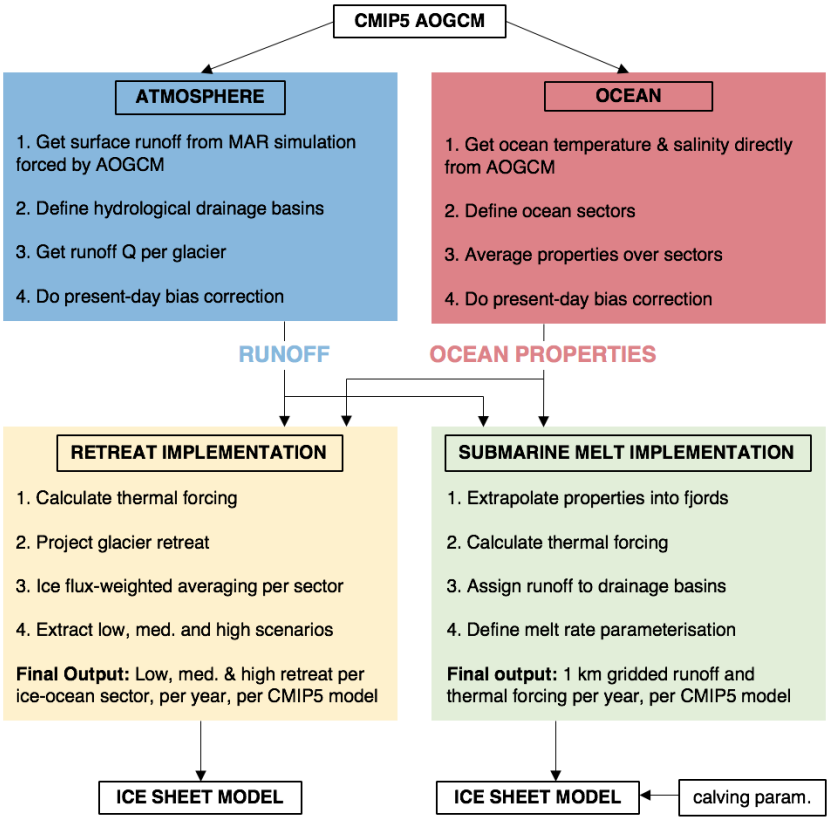

Figure 1. Schematic of proposed approach to use CMIP5 AOGCM output (top) to force Greenland ice sheet models (bottom) under the retreat and submarine melt implementations described in the text. The colored boxes describe the methodology and analysis performed in this paper. Note that the process would be identical for CMIP6 models.

https://doi.org/10.5194/tc-2019-222
Preprint. Discussion started: 26 September 2019

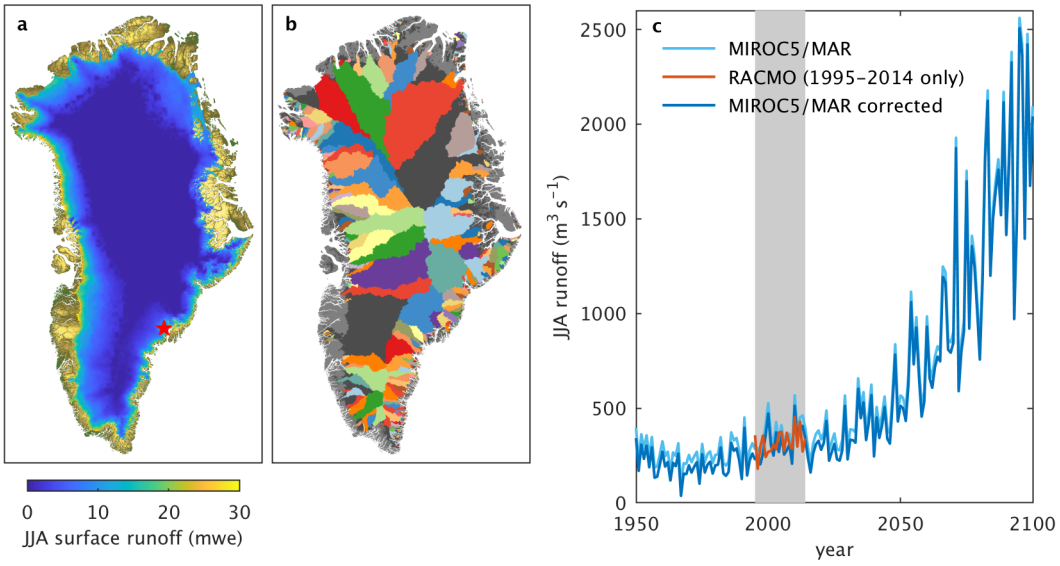

Figure 2. Illustration of atmospheric processing for the MIROC5 RCP8.5 scenario. (a) Simulated June-July-August (JJA) surface runoff in 2100 in the regional climate model MAR3.9.6 forced at its boundaries by MIROC5. (b) Tidewater glacier drainage basins delineated based on the hydropotential defined in Eq. (3). (c) JJA runoff time series for Helheim Glacier in SE Greenland (location shown as red star on (a)). The raw MAR output is in light blue, RACMO during the 1995-2014 baseline period is in red, and the bias-corrected MAR output is in dark blue.

https://doi.org/10.5194/tc-2019-222
Preprint. Discussion started: 26 September 2019

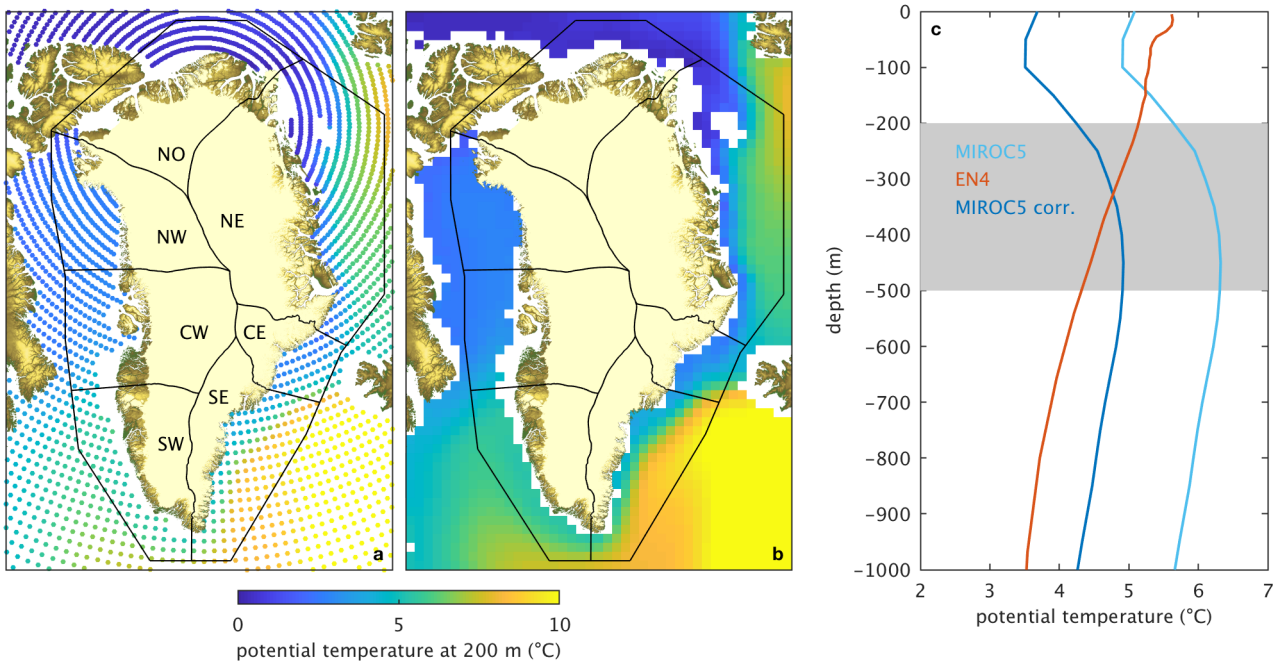

Figure 3. Illustration of ocean processing for the model MIROC5 in an RCP8.5 scenario. (a) Modeled annual mean potential temperature at 200 m in the year 2100, plotted at the resolution of the climate model. The seven ice-ocean sectors over which properties are averaged are also shown and labeled. (b) The same variable, gridded at 50 km resolution for spatial averaging. (c) Ocean temperature bias correction for the SE sector. All three profiles are temporal averages over the 1995-2014 present-day period. The raw MIROC5 output (light blue) is compared to the observational (EN4) profile (red), and is bias-corrected (dark blue), so that the depth-average over the 200-500 m range (shaded grey) agrees with EN4.

https://doi.org/10.5194/tc-2019-222
Preprint. Discussion started: 26 September 2019

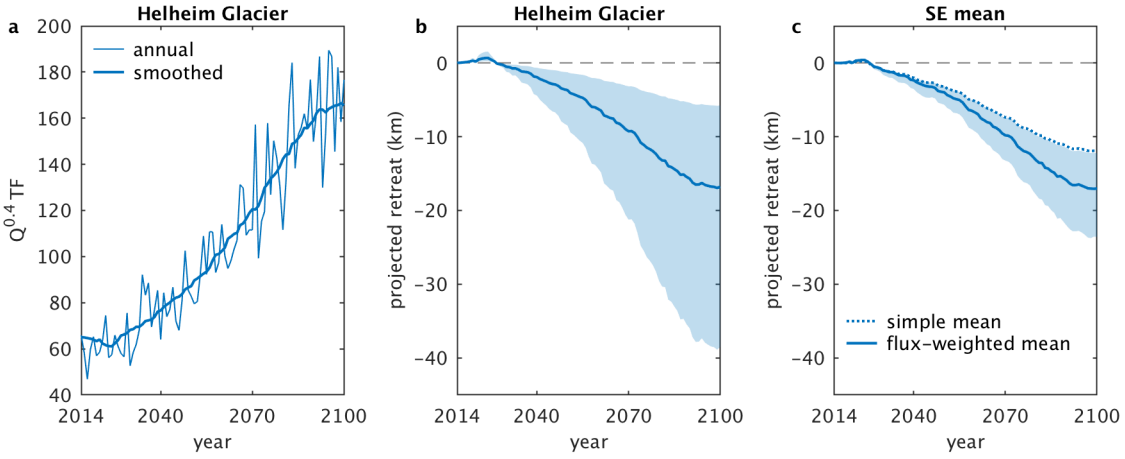

Figure 4. Illustration of retreat implementation processing for MIROC5 under an RCP8.5 scenario. (a) time series of $Q^{0.4}$ TF for Helheim Glacier in SE Greenland, showing annual and 20-year centered mean smoothed values. (b) projected retreat for Helheim Glacier; solid line is the median retreat while the shading denotes the interquartile range of all 10^4 derived retreat trajectories. (c) projected retreat for the SE ice-ocean sector. The dotted line shows the median of the trajectories obtained by taking a simple mean over glaciers, while the solid line and shading show the median and interquartile range of the trajectories obtained by taking an ice flux-weighted mean over glaciers.

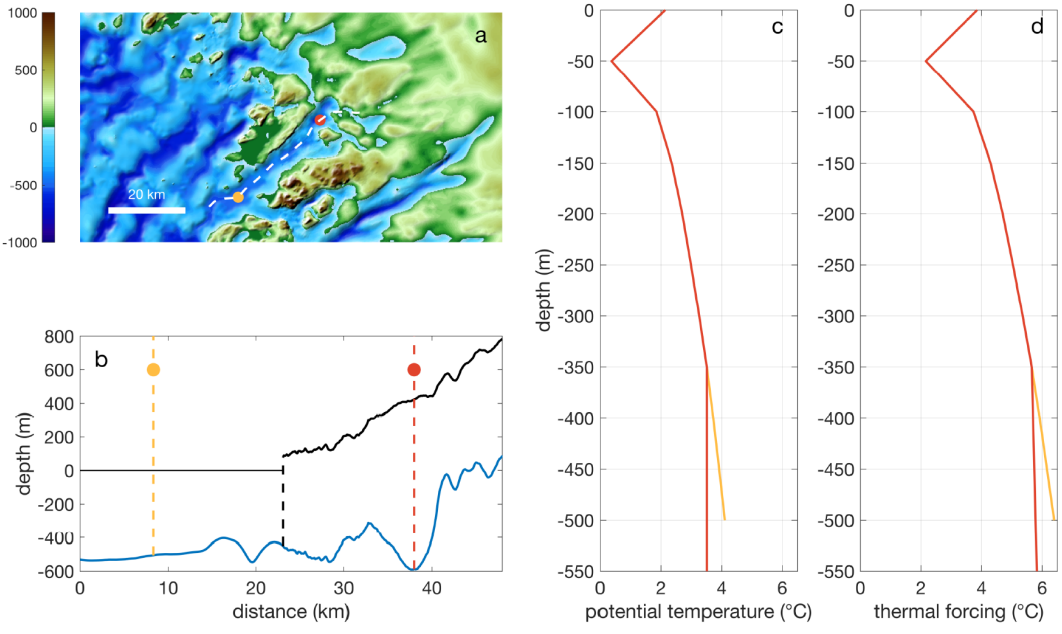

Figure 5. Illustration of ocean property extrapolation for Sverdrup Glacier and fjord, NW Greenland. (a) Overview of regional topography. (b) bathymetry/subglacial topography (blue) and current ice sheet elevation (black) along the flowline shown as the white dashed line in (a). (c) potential temperature profiles and (d) thermal forcing profiles at the locations shown in (a) and (b).

https://doi.org/10.5194/tc-2019-222
Preprint. Discussion started: 26 September 2019

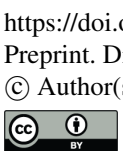

The Cryosphere Discussions
Open Access
EGU

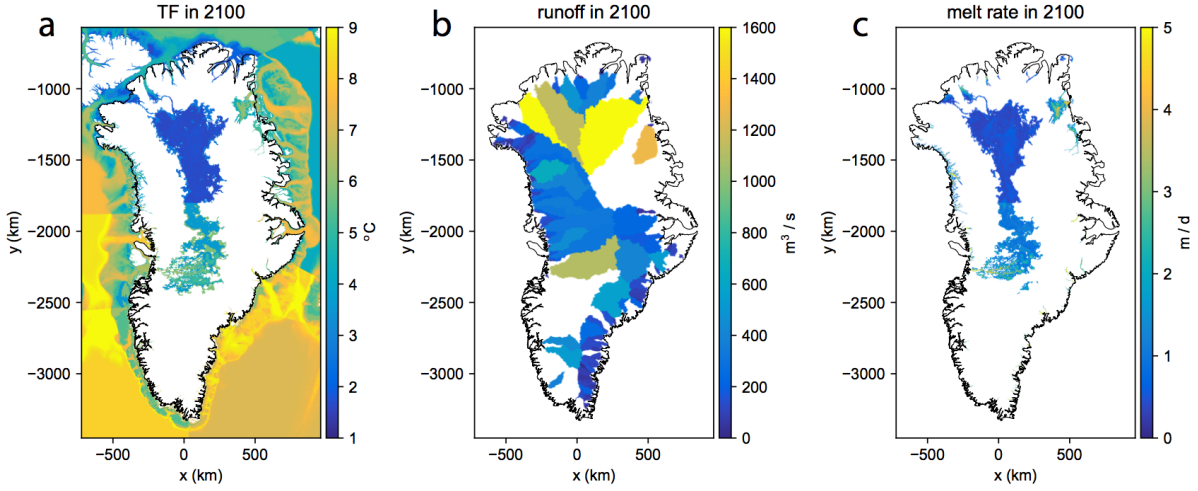

Figure 6. Example of forcing fields in 2100 in the submarine melt implementation, using MIROC5 under an RCP8.5 scenario. (a) ocean thermal forcing, (b) subglacial runoff, and (c) submarine melt rate calculated using the parameterisation in Eq. (1).

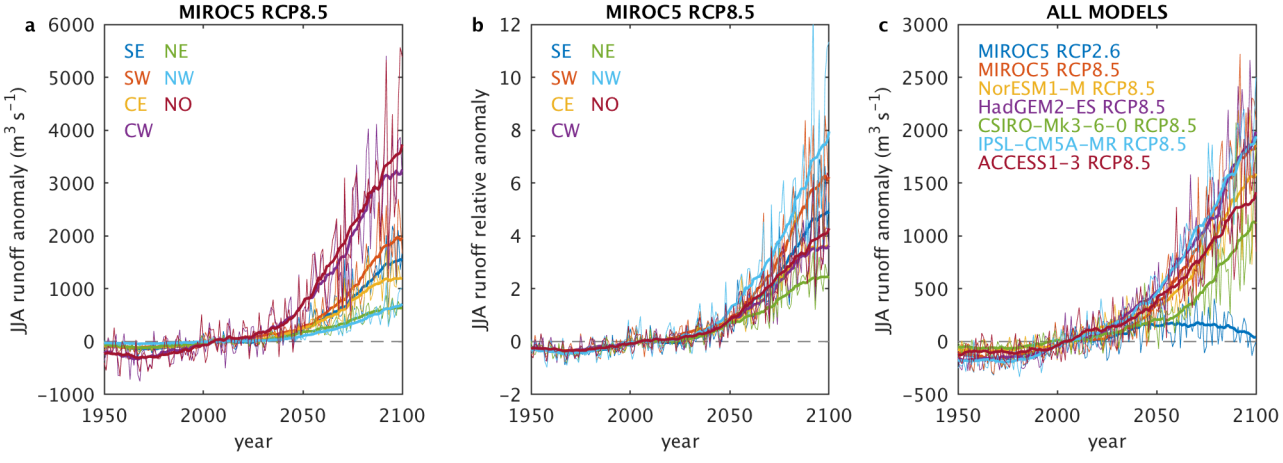

Figure 7. Projected subglacial runoff. For clarity, annual values are plotted as thin lines, and a 20-year running mean is plotted as thicker lines. (a) absolute runoff anomaly (difference from the 1995-2014 mean) by sector in the MIROC5 RCP8.5 simulation. For each sector, the runoff anomaly for the largest glacier by ice flux in that sector is plotted, with the specific glaciers described in the text. (b) runoff relative anomaly (absolute anomaly divided by the 1995-2014 mean). (c) representative runoff anomaly per CMIP AOGCM to illustrate model spread. The representative runoff anomaly is calculated as the mean over the 7 glaciers shown in (a). Full plots for all sectors and models may be found in Figs. S3 and S4.

https://doi.org/10.5194/tc-2019-222
Preprint. Discussion started: 26 September 2019

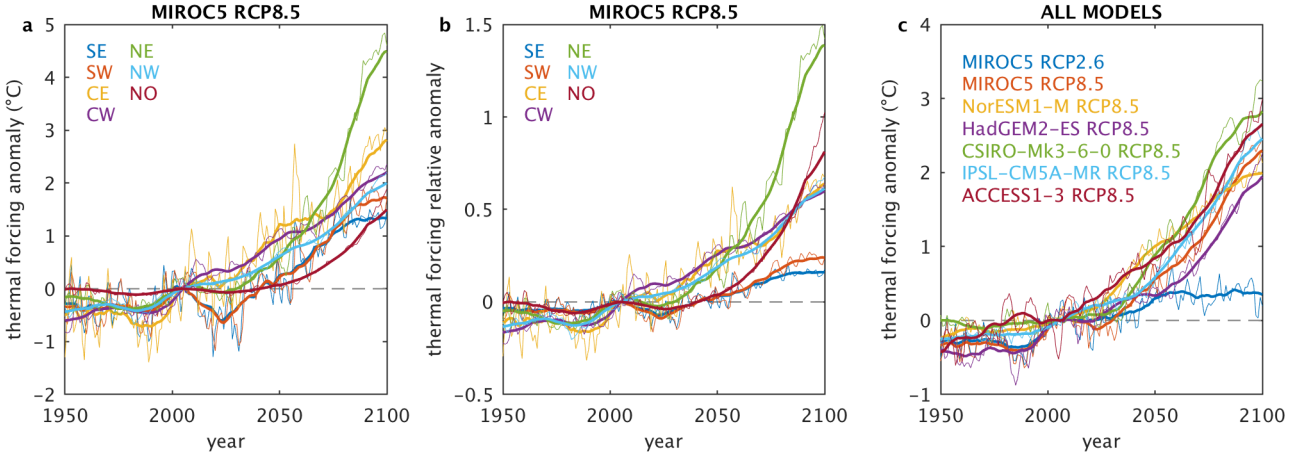

Figure 8. Projected 200-500 m ocean thermal forcing. (a) projected absolute thermal forcing anomaly per ice-ocean sector in the MIROC5 RCP8.5 simulation. (b) relative thermal forcing anomaly. (c) mean thermal forcing over the 7 ice-ocean sectors for each CMIP AOGCM. Full plots for all sectors and all models may be found in Figs. S5 and S6.

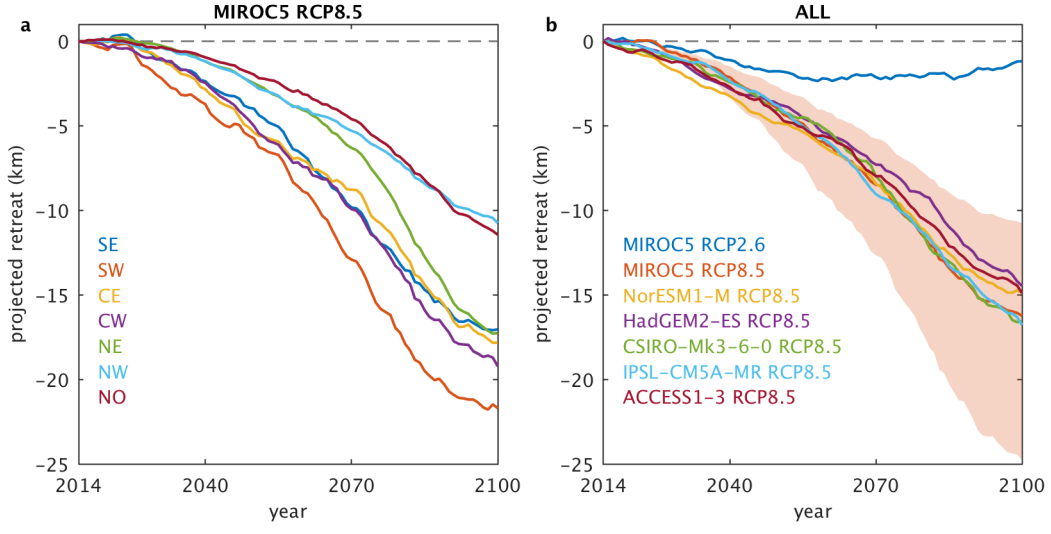

Figure 9. Projected retreat for forcing of Greenland ice sheet models. (a) sector by sector retreat from the MIROC5 RCP8.5 simulation, showing only the medium retreat. (b) retreat in all CMIP AOGCMs considered, where the sectors in (a) are combined according to their present-day relative ice flux (Table S1). Also shown in the shading is the low and high retreat projections for MIROC5 RCP8.5. Note that the ice sheet models are forced on a sector by sector basis, so the projections in (b) are not used to force any models, but are included to give a sense of the multi-model variability. See Fig. S7 for full plots of all projections.

https://doi.org/10.5194/tc-2019-222
Preprint. Discussion started: 26 September 2019

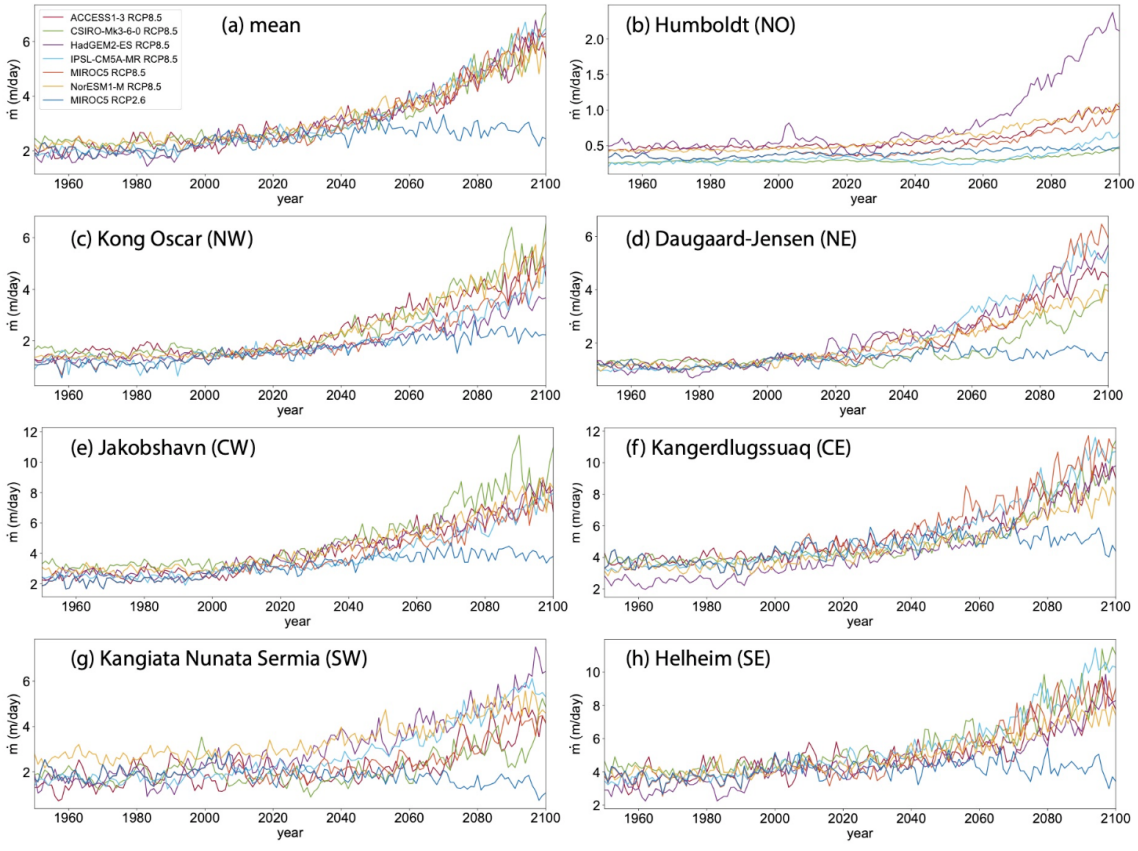

Figure 10. Melt rates in the submarine melt implementation. (a) Mean submarine melt rate over the 7 glaciers that are the largest by ice flux in each of the 7 regions, for the CMIP5 models and scenarios listed in Table 1. (b)-(h) submarine melt rates at the largest glacier by ice flux in each region.

https://doi.org/10.5194/tc-2019-222
Preprint. Discussion started: 26 September 2019

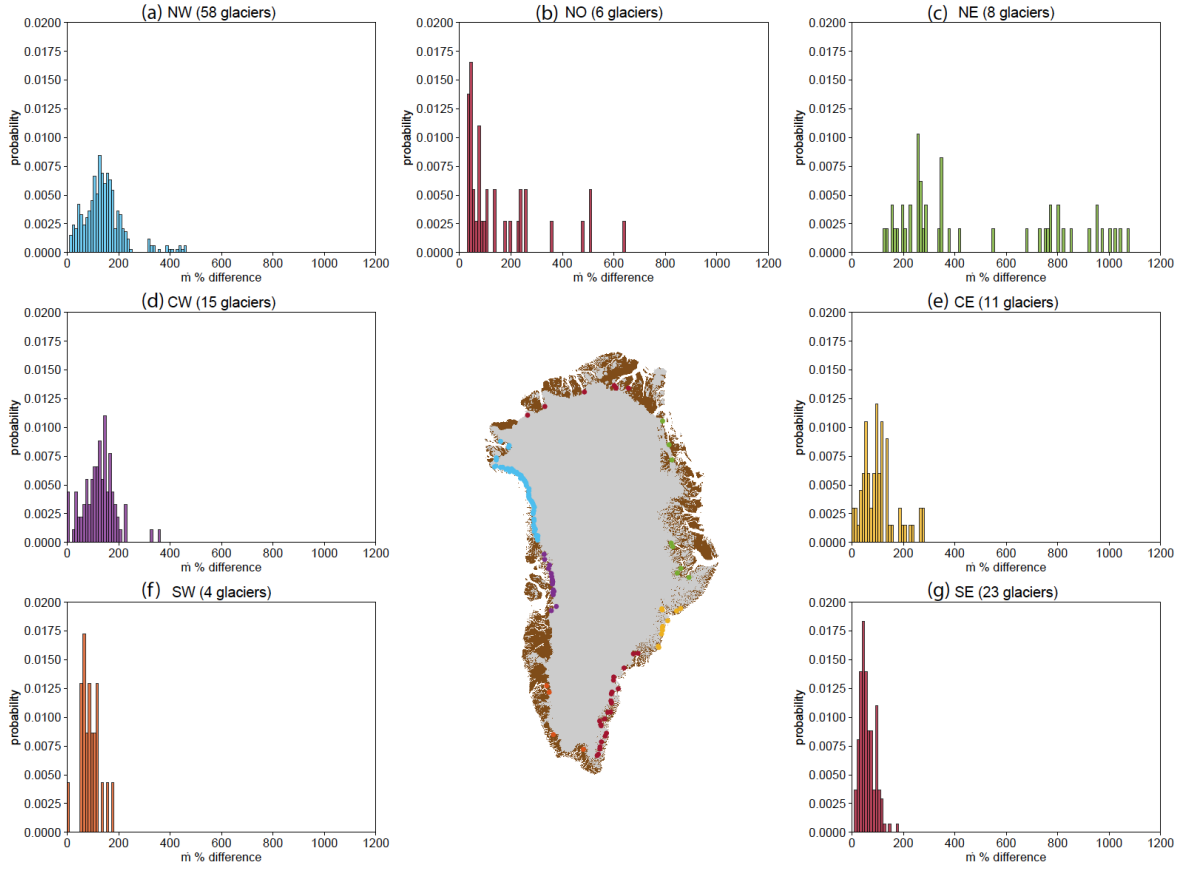

Figure 11. Histograms of percentage differences in glacier submarine melt rates between 1995-2014 and 2081-2100 in the 7 ice-ocean sectors for all 6 CMIP5 RCP8.5 scenarios considered.

https://doi.org/10.5194/tc-2019-222
Preprint. Discussion started: 26 September 2019

Data availability. The bed topography and bathymetry used in this work may be downloaded from https://nsidc.org/data/IDBMG4 (last access September 2019). Information on the RACMO2.3p2 SMB data can be found at http://www.projects.science.uu.nl/iceclimate/models/greenland.php (last access April 2019). EN4.2.1 oceanographic data is available at https://www.metoffice.gov.uk/hadobs/en4/download.html (last access April 2019). CMIP5 model output is available at https://esgf-node.llnl.gov/projects/esgf-llnl/ (last access April 2019). The MAR based future subglacial discharge projections are available on ftp://ftp.climato.be/fettweis/MARv3.9/ISMIP6/GrIS/ (last access April 2019). TEOS-10 routines may be found at http://www.teos-10.org (last access September 2019). Further information on the ISMIP6 project may be found at http://www.climate-cryosphere.org/activities/targeted/ismip6 (last access April 2019). We intend to make all code used to create these projections freely available on the ISMIP6 GitHub page at https://github.com/ismip (last access September 2019). All of the projection datasets described in this paper are freely available from the ISMIP6 ftp server; access can be obtained by emailing ismip6@gmail.com.

Author contributions. DS undertook the majority of the analysis, processing, writing and creation of figures. DF processed past and future runoff and contributed to writing and figures. FS led the ISMIP6 ocean forcing and provided oversight at all stages of the process. HG provided invaluable guidance on the implementation of the described ocean forcing in ice sheet models. CML provided CMIP5 model output and expertise. MM performed the extrapolation of ocean properties into fjords in the submarine melt implementation. XF ran MAR simulations forced by the selected CMIP5 models. SN coordinated the ISMIP6 effort. All authors took part in extensive discussion of the methodology and edited the manuscript.

Competing interests. Xavier Fettweis is a member of the editorial board of the journal. Sophie Nowicki is an editor of the ISMIP6 special issue of The Cryosphere.

Acknowledgements. Donald Slater and Fiamma Straneo were supported by NSF grants 1916566 and 1756272, and by NASA grant NNX17AI03G. Denis Felikson acknowledges financial support from the NASA Postdoctoral Program. Chris Little acknowledges financial support from NSF grant 1513396. Heiko Goelzer has received funding from the programme of the Netherlands Earth System Science Centre (NESSC), financially supported by the Dutch Ministry of Education, Culture and Science (OCW) under grant number 024.002.001. Computational resources for performing MAR future projections have been provided by the Consortium des Équipements de Calcul Intensif (CÉCI), funded by the Fonds de la Recherche Scientifique de Belgique (F.R.S.–FNRS) under grant no. 2.5020.11 and the Tier-1 supercomputer (Zenobe) of the Fédération Wallonie Bruxelles infrastructure funded by the Walloon Region under the grant agreement no. 1117545. Thanks to Brice Noël for RACMO2.3p2 output, to Ellyn Enderlin and Michaela King for ice flux datasets, and to Jeremie Mouginot for sharing ice sheet basin delineations. All members of the ISMIP6 collaboration are thanked for discussions and feedback, notably at ISMIP6 meetings, with particular thanks to Hélène Seroussi, Alice Barthel and Tim Bartholomaus.

https://doi.org/10.5194/tc-2019-222
Preprint. Discussion started: 26 September 2019

References

Amundson, J. M., Fahnestock, M., Truffer, M., Brown, J., Lüthi, M. P., and Motyka, R. J.: Ice mélange dynamics and implications for terminus stability, Jakobshavn Isbræ, Greenland, Journal of Geophysical Research: Earth Surface, 115, https://doi.org/10.1029/2009JF001405, 2010.

Aschwanden, A., Fahnestock, M. A., Truffer, M., Brinkerhoff, D. J., Hock, R., Khroulev, C., Mottram, R., and Khan, S. A.: Contribution of the Greenland Ice Sheet to sea level over the next millennium, Science Advances, 5, https://doi.org/10.1126/sciadv.aav9396, 2019.

Barthel, A., Agosta, C., Little, C. M., Hatterman, T., Jourdain, N. C., Goelzer, H., Nowicki, S., Seroussi, H., Straneo, F., and Bracegirdle, T. J.: CMIP5 model selection for ISMIP6 ice sheet model forcing: Greenland and Antarctica, The Cryosphere Discussions, 2019, 1–34, https://doi.org/10.5194/tc-2019-191, https://www.the-cryosphere-discuss.net/tc-2019-191/, 2019.

Beaird, N. L., Straneo, F., and Jenkins, W.: Export of Strongly Diluted Greenland Meltwater From a Major Glacial Fjord, Geophysical Research Letters, 45, 4163–4170, https://doi.org/10.1029/2018GL077000, 2018.

Beckmann, J., Perrette, M., Beyer, S., Calov, R., Willeit, M., and Ganopolski, A.: Modeling the response of Greenland outlet glaciers to global warming using a coupled flow line-plume model, The Cryosphere, 13, 2281–2301, https://doi.org/10.5194/tc-13-2281-2019, 2019.

Benn, D. I., Astrom, J., Zwinger, T., Todd, J., Nick, F. M., Cook, S., Hulton, N. R. J., and Luckman, A.: Melt-under-cutting and buoyancy-driven calving from tidewater glaciers: new insights from discrete element and continuum model simulations, Journal of Glaciology, 63, 691–702, https://doi.org/10.1017/jog.2017.41, 2017a.

Benn, D. I., Cowton, T., Todd, J., and Luckman, A.: Glacier Calving in Greenland, Current Climate Change Reports, 3, 282–290, https://doi.org/10.1007/s40641-017-0070-1, 2017b.

Bevan, S. L., Luckman, A. J., Benn, D. I., Cowton, T., and Todd, J.: Impact of warming shelf waters on ice mélange and terminus retreat at a large SE Greenland glacier, The Cryosphere, 13, 2303–2315, https://doi.org/10.5194/tc-13-2303-2019, 2019.

Bindschadler, R. A., Nowicki, S., Abe-Ouchi, A., Aschwanden, A., Choi, H., Fastook, J., Granzow, G., Greve, R., Gutowski, G., Herzfeld, U., and et al.: Ice-sheet model sensitivities to environmental forcing and their use in projecting future sea level (the SeaRISE project), Journal of Glaciology, 59, 195–224, https://doi.org/10.3189/2013JoG12J125, 2013.

Bondzio, J. H., Seroussi, H., Morlighem, M., Kleiner, T., Rückamp, M., Humbert, A., and Larour, E. Y.: Modelling calving front dynamics using a level-set method: application to Jakobshavn Isbræ, West Greenland, The Cryosphere, 10, 497–510, https://doi.org/10.5194/tc-10-497-2016, 2016.

Carroll, D., Sutherland, D. A., Shroyer, E. L., Nash, J. D., Catania, G. A., and Stearns, L. A.: Subglacial discharge-driven renewal of tidewater glacier fjords, Journal of Geophysical Research: Oceans, 122, 6611–6629, https://doi.org/10.1002/2017JC012962, 2017.

Catania, G. A., Stearns, L. A., Sutherland, D. A., Fried, M. J., Bartholomaus, T. C., Morlighem, M., Shroyer, E., and Nash, J.: Geometric Controls on Tidewater Glacier Retreat in Central Western Greenland, Journal of Geophysical Research: Earth Surface, 123, 2024–2038, https://doi.org/10.1029/2017JF004499, 2018.

Christoffersen, P., O'Leary, M., Van Angelen, J. H., and Van Den Broeke, M.: Partitioning effects from ocean and atmosphere on the calving stability of Kangerdlugssuaq Glacier, East Greenland, Annals of Glaciology, 53, 249–256, https://doi.org/10.3189/2012AoG60A087, 2012.

Church, J., Clark, P., Cazenave, A., Gregory, J., Jevrejeva, S., Levermann, A., Merrifield, M., Milne, G., Nerem, R., Nunn, P., Payne, A., Pfeffer, W., Stammer, D., and Unnikrishnan, A.: Sea Level Change, book section 13, p. 1137–1216, Cambridge University Press,

Cambridge, United Kingdom and New York, NY, USA, https://doi.org/10.1017/CBO9781107415324.026, www.climatechange2013.org, 2013.

Cowton, T. R., Sole, A. J., Nienow, P. W., Slater, D. A., and Christoffersen, P.: Linear response of east Greenland's tidewater glaciers to ocean/atmosphere warming, Proceedings of the National Academy of Sciences, 115, 7907–7912, https://doi.org/10.1073/pnas.1801769115, 2018.

Enderlin, E. M., Howat, I. M., Jeong, S., Noh, M.-J., van Angelen, J. H., and van den Broeke, M. R.: An improved mass budget for the Greenland ice sheet, Geophysical Research Letters, 41, 866–872, https://doi.org/10.1002/2013GL059010, 2014.

Eyring, V., Bony, S., Meehl, G. A., Senior, C. A., Stevens, B., Stouffer, R. J., and Taylor, K. E.: Overview of the Coupled Model Intercomparison Project Phase 6 (CMIP6) experimental design and organization, Geoscientific Model Development, 9, 1937–1958, https://doi.org/10.5194/gmd-9-1937-2016, 2016.

Fettweis, X., Franco, B., Tedesco, M., van Angelen, J. H., Lenaerts, J. T. M., van den Broeke, M. R., and Gallee, H.: Estimating the Greenland ice sheet surface mass balance contribution to future sea level rise using the regional atmospheric climate model MAR, The Cryosphere, 7, 469–489, https://doi.org/10.5194/tc-7-469-2013, 2013.

Franco, B., Fettweis, X., Lang, C., and Erpicum, M.: Impact of spatial resolution on the modelling of the Greenland ice sheet surface mass balance between 1990-2010, using the regional climate model MAR, The Cryosphere, 6, 695–711, https://doi.org/10.5194/tc-6-695-2012, 2012.

Fried, M. J., Catania, G. A., Bartholomaus, T. C., Duncan, D., Davis, M., Stearns, L. A., Nash, J., E., S., and Sutherland, D.: Distributed subglacial discharge drives significant submarine melt at a Greenland tidewater glacier, Geophysical Research Letters, 42, 9328–9336, https://doi.org/10.1002/2015GL065806, 2015.

Fürst, J. J., Goelzer, H., and Huybrechts, P.: Ice-dynamic projections of the Greenland ice sheet in response to atmospheric and oceanic warming, The Cryosphere, 9, 1039–1062, https://doi.org/10.5194/tc-9-1039-2015, 2015.

Gade, H.: Melting of Ice in Sea Water: A Primitive Model with Application to the Antarctic Ice Shelf and Icebergs, Journal of Physical Oceanography, 9, 189–198, https://doi.org/10.1175/1520-0485(1979)009<0189:MOIISW>2.0.CO;2, 1979.

Gillet-Chaulet, F., Gagliardini, O., Seddik, H., Nodet, M., Durand, G., Ritz, C., Zwinger, T., Greve, R., and Vaughan, D. G.: Greenland ice sheet contribution to sea-level rise from a new-generation ice-sheet model, The Cryosphere, 6, 1561–1576, https://doi.org/10.5194/tc-6-1561-2012, 2012.

Gladish, C. V., Holland, D. M., Rosing-Asvid, A., Behrens, J. W., and Boje, J.: Oceanic Boundary Conditions for Jakobshavn Glacier. Part I: Variability and Renewal of Ilulissat Icefjord Waters, 2001-14, Journal of Physical Oceanography, 45, 3–32, https://doi.org/10.1175/JPO-D-14-0044.1, 2015.

Goelzer, H., Huybrechts, P., Fürst, J., Nick, F., Andersen, M., Edwards, T., Fettweis, X., Payne, A., and Shannon, S.: Sensitivity of Greenland Ice Sheet Projections to Model Formulations, Journal of Glaciology, 59, 733—-749, https://doi.org/10.3189/2013JoG12J182, 2013.

Goelzer, H., Nowicki, S., Edwards, T., Beckley, M., Abe-Ouchi, A., Aschwanden, A., Calov, R., Gagliardini, O., Gillet-Chaulet, F., Golledge, N. R., Gregory, J., Greve, R., Humbert, A., Huybrechts, P., Kennedy, J. H., Larour, E., Lipscomb, W. H., Le clec'h, S., Lee, V., Morlighem, M., Pattyn, F., Payne, A. J., Rodehacke, C., Rückamp, M., Saito, F., Schlegel, N., Seroussi, H., Shepherd, A., Sun, S., van de Wal, R., and Ziemen, F. A.: Design and results of the ice sheet model initialisation experiments initMIP-Greenland: an ISMIP6 intercomparison, The Cryosphere, 12, 1433–1460, https://doi.org/10.5194/tc-12-1433-2018, 2018.

Good, S. A., Martin, M. J., and Rayner, N. A.: EN4: Quality controlled ocean temperature and salinity profiles and monthly objective analyses with uncertainty estimates, Journal of Geophysical Research: Oceans, 118, 6704–6716, https://doi.org/10.1002/2013JC009067, 2013.

https://doi.org/10.5194/tc-2019-222
Preprint. Discussion started: 26 September 2019

Holland, D. M. and Jenkins, A.: Modeling Thermodynamic Ice-Ocean Interactions at the Base of an Ice Shelf, Journal of Physical Oceanography, 29, 1787–1800, https://doi.org/10.1175/1520-0485(1999)029<1787:MTIOIA>2.0.CO;2, 1999.

Holland, D. M., Thomas, R. H., de Young, B., Ribergaard, M. H., and Lyberth, B.: Acceleration of Jakobshavn Isbrae triggered by warm subsurface ocean waters, Nature Geoscience, 1, 659–664, https://doi.org/10.1038/ngeo316, 2008.

How, P., Schild, K. M., Benn, D. I., Noormets, R., Kirchner, N., Luckman, A., Vallot, D., Hulton, N. R. J., and Borstad, C.: Calving controlled by melt-under-cutting: detailed calving styles revealed through time-lapse observations, Annals of Glaciology, pp. 1—-12, https://doi.org/10.1017/aog.2018.28, 2019.

Jackson, R. H., Straneo, F., and Sutherland, D. A.: Externally forced fluctuations in ocean temperature at Greenland glaciers in non-summer months, Nature Geoscience, 7, 503–508, https://doi.org/10.1038/ngeo2186, 2014.

Jackson, R. H., Shroyer, E. L., Nash, J. D., Sutherland, D. A., Carroll, D., Fried, M. J., Catania, G. A., Bartholomaus, T. C., and Stearns, L. A.: Near-glacier surveying of a subglacial discharge plume: Implications for plume parameterizations, Geophysical Research Letters, 44, 6886–6894, https://doi.org/10.1002/2017GL073602, 2017.

Jenkins, A.: Convection-Driven Melting near the Grounding Lines of Ice Shelves and Tidewater Glaciers, Journal of Physical Oceanography, 41, 2279–2294, https://doi.org/10.1175/JPO-D-11-03.1, 2011.

Khan, S. A., Kjeldsen, K. K., Kjaer, K. H., Bevan, S., Luckman, A., Aschwanden, A., Bjørk, A. A., Korsgaard, N. J., Box, J. E., van den Broeke, M. R., van Dam, T. M., and Fitzner, A.: Glacier dynamics at Helheim and Kangerdlugssuaq glaciers, southeast Greenland, since the little ice age, The Cryosphere, 8, 1497–1507, https://doi.org/10.5194/tc-8-1497-2014, 2014.

King, M. D., Howat, I. M., Jeong, S., Noh, M. J., Wouters, B., Noël, B., and van den Broeke, M. R.: Seasonal to decadal variability in ice discharge from the Greenland Ice Sheet, The Cryosphere, 12, 3813–3825, https://doi.org/10.5194/tc-12-3813-2018, 2018.

Krug, J., Durand, G., Gagliardini, O., and Weiss, J.: Modelling the impact of submarine frontal melting and ice mélange on glacier dynamics, The Cryosphere, 9, 989–1003, https://doi.org/10.5194/tc-9-989-2015, 2015.

Luckman, A., Benn, D. I., Cottier, F., Bevan, S., Nilsen, F., and Inall, M.: Calving rates at tidewater glaciers vary strongly with ocean temperature, Nature Communications, 6, https://doi.org/10.1038/ncomms9566, 2015.

Ma, Y. and Bassis, J. N.: The Effect of Submarine Melting on Calving From Marine Terminating Glaciers, Journal of Geophysical Research: Earth Surface, 124, 334–346, https://doi.org/10.1029/2018JF004820, 2019.

Mankoff, K. D., Straneo, F., Cenedese, C., Das, S. B., Richards, C. G., and Singh, H.: Structure and dynamics of a subglacial discharge plume in a Greenlandic fjord, Journal of Geophysical Research: Oceans, 121, 8670–8688, https://doi.org/10.1002/2016JC011764, 2016.

McDougall, T. and Barker, P.: Getting started with TEOS-10 and the Gibbs Seawater (GSW) Oceanographic Toolbox, SCOR/IAPSO WG127, p. 28pp., 2011.

Moon, T., Joughin, I., and Smith, B.: Seasonal to multi-year variability of glacier surface velocity, terminus position, and sea ice/ice melange in northwest Greenland, Journal of Geophysical Research: Earth Surface, https://doi.org/10.1002/2015JF003494, 2015.

Morlighem, M., Williams, C. N., Rignot, E., An, L., Arndt, J. E., Bamber, J. L., Catania, G., Chauché, N., Dowdeswell, J. A., Dorschel, B., Fenty, I., Hogan, K., Howat, I., Hubbard, A., Jakobsson, M., Jordan, T. M., Kjeldsen, K. K., Millan, R., Mayer, L., Mouginot, J., Noël, B. P. Y., O'Cofaigh, C., Palmer, S., Rysgaard, S., Seroussi, H., Siegert, M. J., Slabon, P., Straneo, F., van den Broeke, M. R., Weinrebe, W., Wood, M., and Zinglersen, K. B.: BedMachine v3: Complete Bed Topography and Ocean Bathymetry Mapping of Greenland From Multibeam Echo Sounding Combined With Mass Conservation, Geophysical Research Letters, 44, 11,051–11,061, https://doi.org/10.1002/2017GL074954, 2017.

Morlighem, M., Wood, M., Seroussi, H., Choi, Y., and Rignot, E.: Modeling the response of northwest Greenland to enhanced ocean thermal forcing and subglacial discharge, The Cryosphere, 13, 723–734, https://doi.org/10.5194/tc-13-723-2019, 2019.

Mortensen, J., Lennert, K., Bendtsen, J., and Rysgaard, S.: Heat sources for glacial melt in a sub-Arctic fjord (Godthabsfjord) in contact with the Greenland Ice Sheet, Journal of Geophysical Research: Oceans, 116, https://doi.org/10.1029/2010JC006528, 2011.

Morton, B., Taylor, G., and Turner, J.: Turbulent Gravitational Convection from Maintained and Instantaneous Sources, Proceedings of the Royal Society of London Series a-Mathematical and Physical Sciences, 234, 1–23, https://doi.org/10.1098/rspa.1956.0011, 1956.

Motyka, R. J., Hunter, L., Echelmeyer, K. A., and Connor, C.: Submarine melting at the terminus of a temperate tidewater glacier, LeConte Glacier, Alaska, U.S.A., Annals of Glaciology, 36, 57–65, https://doi.org/10.3189/172756403781816374, 2003.

Mouginot, J., Rignot, E., Bjørk, A. A., van den Broeke, M., Millan, R., Morlighem, M., Noël, B., Scheuchl, B., and Wood, M.: Forty-six years of Greenland Ice Sheet mass balance from 1972 to 2018, Proceedings of the National Academy of Sciences, https://doi.org/10.1073/pnas.1904242116, 2019.

Moyer, A. N., Nienow, P. W., Gourmelen, N., Sole, A. J., Slater, D. A., Truffer, M., and Fahnestock, M.: Spatio-temporal variations in seasonal ice tongue submarine melt rate at a tidewater glacier in southwest Greenland, Journal of Glaciology, 65, 523–530, https://doi.org/10.1017/jog.2019.27, 2019.

Murray, T., Scharrer, K., Selmes, N., Booth, A. D., James, T. D., Bevan, S. L., Bradley, J., Cook, S., Cordero Llana, L., Drocourt, Y., Dyke, L., Goldsack, A., Hughes, A. L., Luckman, A. J., and McGovern, J.: Extensive retreat of Greenland tidewater glaciers, 2000-2010, Arctic, Antarctica, and Alpine Research, 47, 427–447, https://doi.org/10.1657/AAAR0014-049, 2015.

Nick, F. M., Vieli, A., Howat, I. M., and Joughin, I.: Large-scale changes in Greenland outlet glacier dynamics triggered at the terminus, Nature Geoscience, 2, 110–114, https://doi.org/10.1038/ngeo394, 2009.

Nick, F. M., Vieli, A., Andersen, M. L., Joughin, I., Payne, A., Edwards, T. L., Pattyn, F., and van de Wal, R. S. W.: Future sea-level rise from Greenland's main outlet glaciers in a warming climate, Nature, 497, 235–238, https://doi.org/10.1038/nature12068, 2013.

Noël, B., van de Berg, W. J., van Wessem, J. M., van Meijgaard, E., van As, D., Lenaerts, J. T. M., Lhermitte, S., Kuipers Munneke, P., Smeets, C. J. P. P., van Ulft, L. H., van de Wal, R. S. W., and van den Broeke, M. R.: Modelling the climate and surface mass balance of polar ice sheets using RACMO2 – Part 1: Greenland (1958–2016), The Cryosphere, 12, 811–831, https://doi.org/10.5194/tc-12-811-2018, 2018.

Nowicki, S., Bindschadler, R. A., Abe-Ouchi, A., Aschwanden, A., Bueler, E., Choi, H., Fastook, J., Granzow, G., Greve, R., Gutowski, G., Herzfeld, U., Jackson, C., Johnson, J., Khroulev, C., Larour, E., Levermann, A., Lipscomb, W. H., Martin, M. A., Morlighem, M., Parizek, B. R., Pollard, D., Price, S. F., Ren, D., Rignot, E., Saito, F., Sato, T., Seddik, H., Seroussi, H., Takahashi, K., Walker, R., and Wang, W. L.: Insights into spatial sensitivities of ice mass response to environmental change from the SeaRISE ice sheet modeling project I: Antarctica, Journal of Geophysical Research: Earth Surface, 118, 1002–1024, https://doi.org/10.1002/jgrf.20081, 2013a.

Nowicki, S., Bindschadler, R. A., Abe-Ouchi, A., Aschwanden, A., Bueler, E., Choi, H., Fastook, J., Granzow, G., Greve, R., Gutowski, G., Herzfeld, U., Jackson, C., Johnson, J., Khroulev, C., Larour, E., Levermann, A., Lipscomb, W. H., Martin, M. A., Morlighem, M., Parizek, B. R., Pollard, D., Price, S. F., Ren, D., Rignot, E., Saito, F., Sato, T., Seddik, H., Seroussi, H., Takahashi, K., Walker, R., and Wang, W. L.: Insights into spatial sensitivities of ice mass response to environmental change from the SeaRISE ice sheet modeling project II: Greenland, Journal of Geophysical Research: Earth Surface, 118, 1025–1044, https://doi.org/10.1002/jgrf.20076, 2013b.

Nowicki, S. M. J., Payne, A., Larour, E., Seroussi, H., Goelzer, H., Lipscomb, W., Gregory, J., Abe-Ouchi, A., and Shepherd, A.: Ice Sheet Model Intercomparison Project (ISMIP6) contribution to CMIP6, Geoscientific Model Development, 9, 4521–4545, https://doi.org/10.5194/gmd-9-4521-2016, 2016.

Peano, D., Colleoni, F., Quiquet, A., and Masina, S.: Ice flux evolution in fast flowing areas of the Greenland ice sheet over the 20th and 21st centuries, Journal of Glaciology, 63, 499—-513, https://doi.org/10.1017/jog.2017.12, 2017.

Price, S. F., Payne, A. J., Howat, I. M., and Smith, B. E.: Committed sea-level rise for the next century from Greenland ice sheet dynamics during the past decade, Proceedings of the National Academy of Sciences, 108, 8978–8983, https://doi.org/10.1073/pnas.1017313108, 2011.

Rignot, E. and Kanagaratnam, P.: Changes in the Velocity Structure of the Greenland Ice Sheet, Science, 311, 986–990, https://doi.org/10.1126/science.1121381, 2006.

Rignot, E., Fenty, I., Xu, Y., Cai, C., and Kemp, C.: Undercutting of marine-terminating glaciers in West Greenland, Geophysical Research Letters, 42, 5909–5917, https://doi.org/10.1002/2015GL064236, 2015.

Rignot, E., Xu, Y., Menemenlis, D., Mouginot, J., Scheuchl, B., Li, X., Morlighem, M., Seroussi, H., den Broeke, M. v., Fenty, I., Cai, C., An, L., and Fleurian, B. d.: Modeling of ocean-induced ice melt rates of five west Greenland glaciers over the past two decades, Geophysical Research Letters, 43, 6374–6382, https://doi.org/10.1002/2016GL068784, 2016.

Robel, A. A.: Thinning sea ice weakens buttressing force of iceberg mélange and promotes calving, Nature Communications, 8, https://doi.org/10.1038/ncomms14596, 2017.

Schaffer, J., von Appen, W.-J., Dodd, P. A., Hofstede, C., Mayer, C., de Steur, L., and Kanzow, T.: Warm water pathways toward Nioghalvfjerdsfjorden Glacier, Northeast Greenland, Journal of Geophysical Research: Oceans, 122, 4004–4020, https://doi.org/10.1002/2016JC012462, 2017.

Schwanghart, W. and Scherler, D.: Short Communication: TopoToolbox 2 - MATLAB-based software for topographic analysis and modeling in Earth surface sciences, Earth Surface Dynamics, 2, 1–7, https://doi.org/10.5194/esurf-2-1-2014, 2014.

Shepherd, A., Ivins, E. R., A, G., Barletta, V. R., Bentley, M. J., Bettadpur, S., Briggs, K. H., Bromwich, D. H., Forsberg, R., Galin, N., Horwath, M., Jacobs, S., Joughin, I., King, M. A., Lenaerts, J. T. M., Li, J., Ligtenberg, S. R. M., Luckman, A., Luthcke, S. B., McMillan, M., Meister, R., Milne, G., Mouginot, J., Muir, A., Nicolas, J. P., Paden, J., Payne, A. J., Pritchard, H., Rignot, E., Rott, H., Sørensen, L. S., Scambos, T. A., Scheuchl, B., Schrama, E. J. O., Smith, B., Sundal, A. V., Angelen, J. H. v., Berg, W. J. v. d., Broeke, M. R. v. d., Vaughan, D. G., Velicogna, I., Wahr, J., Whitehouse, P. L., Wingham, D. J., Yi, D., Young, D., and Zwally, H. J.: A Reconciled Estimate of Ice-Sheet Mass Balance, Science, 338, 1183–1189, https://doi.org/10.1126/science.1228102, 2012.

Shreve, R. L.: Movement of water in glaciers, Journal of Glaciology, 11, 205–214, https://doi.org/10.3198/1972JoG11-62-205-214, 1972.

Slater, D., Straneo, F., Felikson, D., Little, C., Goelzer, H., Fettweis, X., and Holte, J.: Past and future response of Greenland's tidewater glaciers to submarine melting, The Cryosphere Discussions, 2019, 1–32, https://doi.org/10.5194/tc-2019-98, https://www.the-cryosphere-discuss.net/tc-2019-98/, 2019.

Slater, D. A., Goldberg, D. N., Nienow, P. W., and Cowton, T. R.: Scalings for submarine melting at tidewater glaciers from buoyant plume theory, Journal of Physical Oceanography, 46, 1839–1855, https://doi.org/10.1175/JPO-D-15-0132.1, 2016.

Slater, D. A., Straneo, F., Das, S. B., Richards, C. G., Wagner, T. J. W., and Nienow, P. W.: Localized Plumes Drive Front-Wide Ocean Melting of A Greenlandic Tidewater Glacier, Geophysical Research Letters, 45, 12 350–12 358, https://doi.org/10.1029/2018GL080763, 2018.

Straneo, F. and Heimbach, P.: North Atlantic warming and the retreat of Greenland's outlet glaciers, Nature, 504, 36–43, https://doi.org/10.1038/nature12854, 2013.

Straneo, F., Hamilton, G. S., Sutherland, D. A., Stearns, L. A., Davidson, F., Hammill, M. O., Stenson, G. B., and Rosing-Asvid, A.: Rapid circulation of warm subtropical waters in a major glacial fjord in East Greenland, Nature Geoscience, 3, 182–186, https://doi.org/10.1038/ngeo764, 2010.

Straneo, F., Curry, R. G., Sutherland, D. A., Hamilton, G. S., Cenedese, C., Vage, K., and Stearns, L. A.: Impact of fjord dynamics and glacial runoff on the circulation near Helheim Glacier, Nature Geoscience, 4, 322–327, https://doi.org/10.1038/ngeo1109, 2011.

Sutherland, D. A., Jackson, R. H., Kienholz, C., Amundson, J. M., Dryer, W. P., Duncan, D., Eidam, E. F., Motyka, R. J., and Nash, J. D.: Direct observations of submarine melt and subsurface geometry at a tidewater glacier, Science, 365, 369–374, https://doi.org/10.1126/science.aax3528, 2019.

Taylor, K. E., Stouffer, R. J., and Meehl, G. A.: An Overview of CMIP5 and the Experiment Design, Bulletin of the American Meteorological Society, 93, 485–498, https://doi.org/10.1175/BAMS-D-11-00094.1, 2012.

Todd, J., Christoffersen, P., Zwinger, T., Raback, P., Chauche, N., Benn, D., Luckman, A., Ryan, J., Toberg, N., Slater, D., and Hubbard, A.: A Full-Stokes 3D Calving Model applied to a large Greenlandic Glacier, Journal of Geophysical Research: Earth Surface, 123, 410–432, https://doi.org/10.1002/2017JF004349, 2018.

van den Broeke, M. R., Enderlin, E. M., Howat, I. M., Kuipers Munneke, P., Noel, B. P. Y., van de Berg, W. J., van Meijgaard, E., and Wouters, B.: On the recent contribution of the Greenland ice sheet to sea level change, The Cryosphere, 10, 1933–1946, https://doi.org/10.5194/tc-10-1933-2016, 2016.

Wagner, T. J. W., Straneo, F., Richards, C. G., Slater, D. A., Stevens, L. A., Das, S. B., and Singh, H.: Large spatial variations in the flux balance along the front of a Greenland tidewater glacier, The Cryosphere, 13, 911–925, https://doi.org/10.5194/tc-13-911-2019, https://www.the-cryosphere.net/13/911/2019/, 2019.

Wilson, N., Straneo, F., and Heimbach, P.: Satellite-derived submarine melt rates and mass balance (2011–2015) for Greenland's largest remaining ice tongues, The Cryosphere, 11, 2773–2782, https://doi.org/10.5194/tc-11-2773-2017, 2017.

Wood, M., Rignot, E., Fenty, I., Menemenlis, D., Millan, R., Morlighem, M., Mouginot, J., and Seroussi, H.: Ocean-Induced Melt Triggers Glacier Retreat in Northwest Greenland, Geophysical Research Letters, 45, 8334–8342, https://doi.org/10.1029/2018GL078024, 2018.

Xu, Y., Rignot, E., Fenty, I., Menemenlis, D., and Flexas, M. M.: Subaqueous melting of Store Glacier, West Greenland from three-dimensional, high-resolution numerical modeling and ocean observations, Geophysical Research Letters, 40, 4648–4653, https://doi.org/10.1002/grl.50825, 2013.

Yin, J., Overpeck, J. T., Griffies, S. M., Hu, A., Russell, J. L., and Stouffer, R. J.: Different magnitudes of projected subsurface ocean warming around Greenland and Antarctica, Nature Geoscience, 4, 524–528, https://doi.org/10.1038/ngeo1189, 2011.